Resonance phenomenon for the Galerkin-truncated Burgers and Euler equations

Samriddhi Sankar Ray,[1] Uriel Frisch,[1] Sergei Nazarenko,[2] and Takeshi Matsumoto[3]

[1]*UNS, CNRS, OCA, Lab. Cassiopée, B.P. 4229, 06304 Nice Cedex 4, France*[*]
[2]*University of Warwick, Mathematics Institute, Coventry CV4 7AL, UK*
[3]*Dept. of Physics, Kyoto University, Kitashirakawa Oiwakecho Sakyoku, Kyoto 606-8502, Japan*

It is shown that the solutions of inviscid hydrodynamical equations with suppression of all spatial Fourier modes having wavenumbers in excess of a threshold $K_{\rm G}$ exhibit unexpected features. The study is carried out for both the one-dimensional Burgers equation and the two-dimensional incompressible Euler equation. For large $K_{\rm G}$ and smooth initial conditions, the first symptom of truncation, a localized short-wavelength oscillation which we call a "tyger", is caused by a resonant interaction between fluid particle motion and truncation waves generated by small-scale features (shocks, layers with strong vorticity gradients, etc). These tygers appear when complex-space singularities come within one Galerkin wavelength $\lambda_{\rm G} = 2\pi/K_{\rm G}$ from the real domain and typically arise far away from preexisting small-scale structures at locations whose velocities match that of such structures. Tygers are weak and strongly localized at first—in the Burgers case at the time of appearance of the first shock their amplitudes and widths are proportional to ${K_{\rm G}}^{-2/3}$ and ${K_{\rm G}}^{-1/3}$ respectively—but grow and eventually invade the whole flow. They are thus the first manifestations of the thermalization predicted by T.D. Lee in 1952.

The sudden dissipative anomaly—the presence of a finite dissipation in the limit of vanishing viscosity after a finite time $t_\star$–, which is well known for the Burgers equation and sometimes conjectured for the 3D Euler equation, has as counterpart, in the truncated case, the ability of tygers to store a finite amount of energy in the limit $K_{\rm G} \to \infty$. This leads to Reynolds stresses acting on scales larger than the Galerkin wavelength and thus prevents the flow from converging to the inviscid-limit solution. There are indications that it may eventually be possible to purge the tygers and thereby to recover the correct inviscid-limit behaviour.

PACS numbers: 05.20.Jj, 05.45.-a, 47.27.Jv

I. INTRODUCTION AND FORMULATION

When the motion of a fluid is described at the microscopic level, a *conservative* Hamiltonian formulation is appropriate and statistical steady states can be described using Gibbs ensembles. At the macroscopic level, however, one obtains a *dissipative* hydrodynamical description because macroscopic motion can be irreversibly degraded into thermal molecular motion. Curiously, T.D. Lee observed that, starting from the hydrodynamical or magnetohydrodynamical equations for an *ideal fluid*, one can obtain a conservative dynamical system to which Gibbsian statistical mechanics becomes applicable [1]. For this he used a Galerkin truncation of the equations, a procedure that keeps only a finite number of spatial Fourier harmonics. For the case of the Galerkin-truncated 3D incompressible Euler equation, Lee obtained thermalized equilibrium statistical states having an equipartition of kinetic energy among all the Fourier harmonics and thus a k^2 energy spectrum. This is very far from the spectrum of fully developed turbulence as observed experimentally, which could lead one to believe that Galerkin truncation applied to the Euler equation cannot tell us anything about the dissipative states of turbulence.

Kraichnan was the first to think otherwise. Considerations of the Galerkin-truncated equilibria of the 2D Euler equation played an important role in his conjecture about an inverse energy cascade [2, 3]. In 1989 he and S. Chen went much further and wrote ([4], p. 162):

> the truncated Euler system can imitate NS [Navier-Stokes] fluid: the high-wavenumber degrees of freedom act like a thermal sink into which the energy of low-wave-number modes excited above equilibrium is dissipated. In the limit where the sink wavenumbers are very large compared with the anomalously excited wavenumbers, this dynamical damping acts precisely like a molecular viscosity.

Supporting evidence was found in 2005 with very-high-resolution spectral simulations of the 3D Galerkin-truncated Euler equation that showed the following: when initial conditions are used that have mostly low-wavenumber modes, the solutions have long-lasting transients in which only the high-wavenumber modes are thermalized, while the lower-wavenumber modes behave in a way similar to that for viscous high-Reynolds-number flow [5]. This seems to hold not only when the low-wavenumber modes are weak (as implicitly assumed by Kraichnan who invoked the fluctuation-dissipation relations) but also in the strong turbulence regime that displays a K41-type inertial range. One possible interpretation is that the thermalized modes act as a kind of artificial molecular world, thereby allowing dissipative (Navier–Stokes) dynamics for the lower-wavenumber modes.

We understand far too little about the mathematics of the 3D Euler and Navier–Stokes equations to start a serious analytical investigation of what happens to solutions of the Galerkin-truncated 3D Euler equation when $K_{\rm G} \to \infty$. However, such matters may be within reach for the one-dimensional inviscid Burgers equation, a well-understood problem in the ab-

[*]SSR: also at Centre for Condensed Matter Theory, Department of Physics, Indian Institute of Science, Bangalore, India

sence of truncation. Even in that "simple" case, the behavior at large $K_{\rm G}$ is far from obvious. Indeed, there are known instances where an energy-conserving modification of the inviscid Burgers equation with a small parameter is found not to converge [35] to the inviscid limit [6, 7] (see also [8]). Hence caution is needed and we shall discuss this issue further.

There is also an important practical reason to be interested in Galerkin-truncated hydrodynamics. Spectral methods (and their pseudo-spectral variants) are among the most precise methods for the numerical integration of hydrodynamical equations [9]. By necessity, a finite resolution must then be used. In other words one integrates not the full hydrodynamical equations but their Galerkin-truncated modifications. If the high-wavenumber modes are sufficiently damped by viscous dissipation the difference may be extremely small. Yet the desire to push the Reynolds number can lead to serious truncation errors. Furthermore in investigations of the blow-up problem for the 3D Euler equation (cf., e.g., Refs. [10, 11] and references therein) it is important to be able to distinguish genuine blow-up from truncation effects.

We had one additional reason to investigate what exactly are the consequences of Galerkin truncation. M.E. Brachet (private communication 2007) informed us about a strange phenomenon observed when Galerkin truncation is used in conjunction with the one-dimensional inviscid Burgers equation

$$\partial_t u + u\partial_x u = 0; \qquad u(x,0) = u_0(x). \tag{1}$$

The initial condition $u_0(x)$ has just a few Fourier harmonics and the number of retained Fourier modes is large. The first symptom of Galerkin truncation found by Brachet was a spurious oscillation in physical space, seemingly born not at all where one would expect it, namely in the neighborhood of genuine small-scale structures such as shocks and their precursors called preshocks, but completely "out of the blue" at a place having no particular small-scale activity, as illustrated in Fig. 1.

In this paper we shall understand why this happens, both for the Burgers equation and for the Euler equation (so far mostly in 2D). The phenomenon is here called *tyger* after William Blake's poem for reasons given later. Before proceeding to explain the organization of the paper, it is useful to define our Galerkin-truncated problem more precisely for the case of the Burgers equation (the 2D Euler case will be formulated in Sec. II C). We restrict ourselves to 2π periodic solutions which can be expanded in a Fourier series

$$u(x) = \sum_{k=0,\pm1,\pm2\ldots} \mathrm{e}^{\mathrm{i}kx}\hat{u}_k. \tag{2}$$

Let $K_{\rm G}$ be a positive integer, here called the Galerkin truncation wavenumber. We define the Galerkin projector $\mathrm{P}_{K_{\rm G}}$ as the low-pass filter which sets to zero all Fourier components with wavenumbers $|k| > K_{\rm G}$. In other words

$$\mathrm{P}_{K_{\rm G}} u(x) = \sum_{|k|\le K_{\rm G}} \mathrm{e}^{\mathrm{i}kx}\hat{u}_k. \tag{3}$$

The (untruncated) inviscid Burgers equation, written in conservation form, is

$$\partial_t u + \partial_x(u^2/2) = 0; \qquad u(x,0) = u_0(x). \tag{4}$$

The associated Galerkin-truncated (inviscid) Burgers equation whose solution is denoted $v(x,t)$ is obtained by applying the low-pass filter to both the initial condition and to the nonlinear term [15]. It reads

$$\partial_t v + \mathrm{P}_{K_{\rm G}}\partial_x(v^2/2) = 0; \qquad v_0 = \mathrm{P}_{K_{\rm G}} u_0. \tag{5}$$

As is well known, the gradient $\partial_x u$ of the solution to the inviscid Burgers equation with smooth initial data typically blows up after a finite time $t_\star$. At $t_\star$ the solution u has a cubic-root singularity, called a preshock [16, 17]. Beyond $t_\star$ the solution can be continued by introducing a small viscous term into the r.h.s. of (1); in the limit of vanishing viscosity one obtains what we here call the inviscid-limit solution, which has one or several shocks [12]. This is a generalized solution which satisfies the inviscid Burgers equation only in a weak sense. The inviscid-limit solution has a *dissipative anomaly*, i.e., it dissipates energy even in the limit of vanishing viscosity. In contrast, the solution to the Galerkin-truncated equation (5) stays smooth and conserves energy forever.

This paper has two main parts: Sec. II deals with the numerical exploration of the tyger phenomenon and includes soft phenomenological interpretations of our various findings. More specifically, in Sec. II A we identify the resonant particle-wave interaction mechanism responsible for the birth of tygers. In Sec. II B we present the whole temporal scenario from the birth of tygers to full thermalization. In Sec.II C we show that the 2D incompressible Euler equation also gives rise to tygers by a mechanism similar to what we find for the Burgers equation. In Sec. II D we investigate the energetics (dissipative anomaly) and the issue of the (weak) limit of the truncated solutions when $K_{\rm G} \to \infty$. Sec. III is restricted to the birth of tygers for the Burgers equation; it involves state-of-the-art simulations of the scaling properties with $K_{\rm G}$ up to $40,000$ and also a fair amount of analytic theory. Open problems and conclusions are presented in Sec. IV. There are four technical appendices.

II. SIMULATIONS AND PHENOMENOLOGY

A. Tygers and resonance

Henceforth, when we write about a/the "untruncated solution of the Burgers equation", without specifying more, it is the inviscid limit of the untrucated Burgers equation which is understood. A particularly simple 2π-periodic solution of the Burgers equation is obtained with the initial condition

$$u_0(x) = \sin x, \tag{6}$$

which has two stagnation (zero-velocity) points, $x = 0$ with positive strain (gradient) and $x = \pi$ with negative strain. The latter gives rise to a cubic-root preshock singularity at the time

$t = t_\star = 1$ [36]. Hereafter the initial condition (6) and its space-translates will be referred to as "single-mode initial condition".

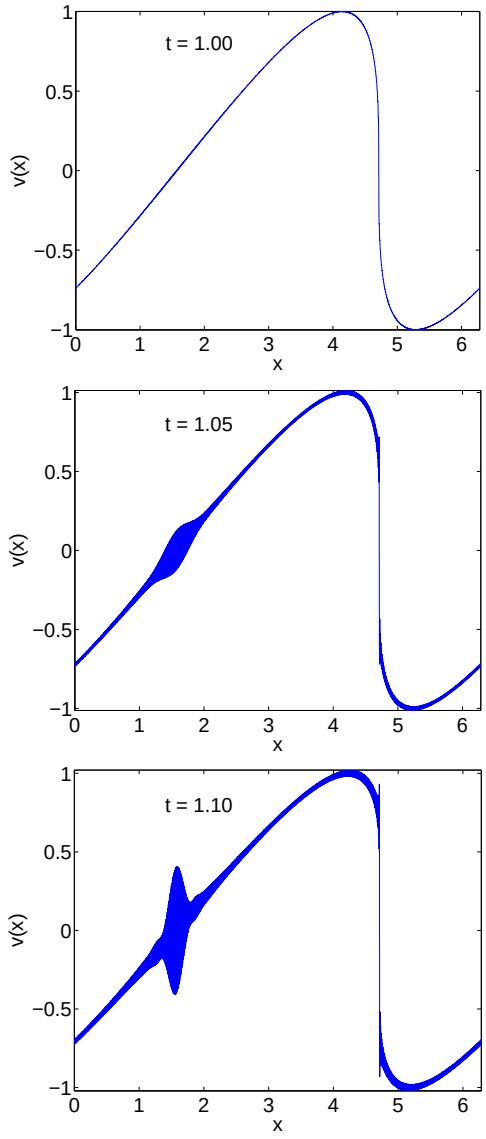

FIG. 1: (Color online) Growth of a tyger in the solution of the inviscid Burgers equation with initial condition $v_0(x) = \sin(x - \pi/2)$ (to avoid graphical edge effects). Galerkin truncation at $K_{\rm G} = 700$. Number of collocation points $N = 16,384$. Output time as labelled. Observe that the bulge appears far from the place of birth of the shock. In the PDF online version of this paper all high-resolution figures are fully zoomable.

With this initial condition, the tyger phenomenon is particularly simple to observe. Fig. 1 shows the solution of the truncated Burgers equation with $K_{\rm G} = 700$ at $t = t_\star$ and at slightly later times [37]. Near $x = 3\pi/2 \approx 4.712$ the cubic-root preshock singularity at $t_\star$ and the shock beyond that time are standard features. The new one is the "tyger", a growing bulge near the positive-strain stagnation point [38]. A more detailed view is shown in Fig. 2 which shows the *discrepancy* $\tilde{u} \equiv v - u$ between the truncated solution and the untruncated one, and zooms into the tyger region and the preshock regions at time $t_\star$ and shortly thereafter. The bulges seen consist basically of oscillations at the *Galerkin wavelength*

$$\lambda_{\rm G} \equiv \frac{2\pi}{K_{\rm G}}. \tag{7}$$

with a localized envelope function which is symmetrical around the center; this symmetry will actually be destroyed later by nonlinearity, as we shall see in Sec. II B.

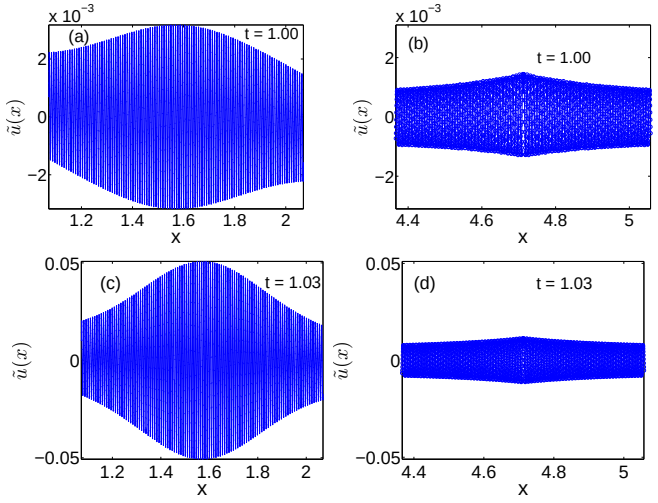

FIG. 2: (Color online) Close-up views of the discrepancy $\tilde{u}(x)$ at time $t = t_\star = 1$ and $t = 1.03$ in the tyger regions (panels (a) and (c), respectively) and in the preshock region (panels (b) and (d), respectively). Same conditions as Fig 1. Note that the tyger bulge grows much faster than the preshock bulge.

We now use a multi-mode initial condition

$$u_0(x) = \sin(x) + \sin(2x + 0.9) + \sin(3x), \tag{8}$$

for which the first singularity is at $t_\star = 0.2218$. Simulating the truncated solution, again with $K_{\rm G} = 700$, we see (cf. Fig. 3) that at $t = 0.25$ there is a well-developed shock (near $x = 1.30$), decorated by tygers on each side.

The tygers are centered around points where the velocity equals the half-sum of the limiting velocities when approaching the shock from the left and the right. For the Burgers equation this is precisely the velocity of the shock. Note that there is yet another point (around $x = 3.30$) which has the same velocity but no tyger; it has however a negative strain. Thus tygers appear to be born at points of positive strain having the same velocity as a shock.

We turn now to the phenomenological explanation of the tyger phenomenon, leaving more systematic theory for Sec. III. The presence of the Galerkin truncation projector $\mathrm{P}_{K_{\rm G}}$ makes (5) nonlocal in physical (x) space. A localized strong nonlinearity, such as is present at a preshock or a shock, acts as a source of a *truncation wave* whose spatial dependence is the Fourier transform of the low-pass filter projector [39].

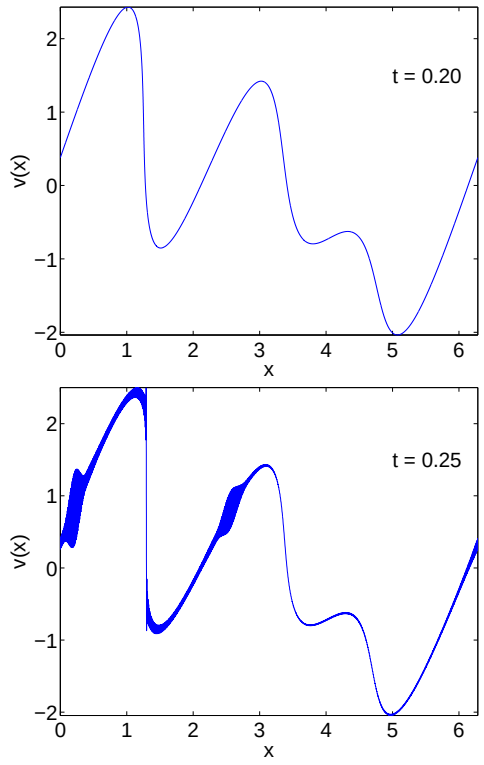

FIG. 3: (Color online) Three-mode initial condition. Other parameters as in Fig. 1. Tygers appear at the points having the same velocity as the shock and positive strain.

More precisely, in physical space the nonlinear term involves a convolution with

$$g_{K_{\rm G}}(x) \equiv \sum_{k=-K_{\rm G}}^{k=K_{\rm G}} {\rm e}^{{\rm i}kx} = \frac{\sin\left(K_{\rm G}+\frac{1}{2}\right)x}{\sin\left(\frac{x}{2}\right)}. \qquad (9)$$

Away from the source (where it is close to a Dirac measure for large $K_{\rm G}$), this "truncation wave" is mostly a plane wave with wavenumber close to $K_{\rm G}$ (see Fig. 4) and thus has a wavelength close to the Galerkin wavelength,

$$\lambda_{\rm G} \equiv \frac{2\pi}{K_{\rm G}}. \qquad (10)$$

Observe that if a preshock/shock is moving with velocity $v_{\rm s}$, the associated truncation wave becomes a progressive wave with phase velocity $v_{\rm s}$.

Away from the shock region, the Burgers equation can be interpreted as describing a particle dynamics: from a Lagrangian point of view, fluid particles just move with their velocity unchanged. In the presence of truncation, those particles which happen to have a velocity equal to the phase velocity of a truncation wave can *resonantly interact* with such waves [40].

Resonant particle-wave interaction is a well known phenomenon. It is used, for example, in plasma physics to explain Landau damping [14]: the near coincidence of the velocity of particles and of the phase velocity of Langmuir wave

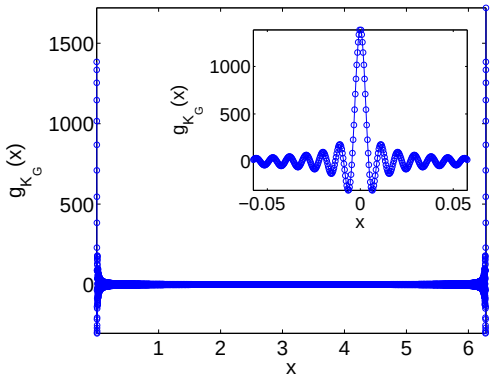

FIG. 4: (Color online) Truncation wave with wavenumber $K_{\rm G} = 700$.

allows efficient interactions between the two. This can lead to wave attenuation (actual Landau damping) or enhancement (beam instability, bump on the tail instability, ...). There are however substantial differences between the Vlasov equation (governing the Landau instability) and the truncated Burgers equation. For example the Langmuir wave evolves through energy transfers via the resonance, a problem which in the linear approximation can be solved by use of the Laplace transform (leading to Landau's rule for a pole-avoiding integration path); in contrast, our truncation waves are completely prescribed by the singularities (preshocks or shocks) and undergo no damping in the linear approximation. Furthermore the linear approximaton does not have an easy analytic solution (cf. Sec. III). In Landau damping, resonant particles get trapped and a characteristic "cat eyes" phase-space distribution with progressively thinning filamentary structure is obtained (cf. Fig. II-1 of [19]). In the truncated Burgers dynamics thinning is arrested by truncation.

The radiation of truncation waves begins only at or close to the time of formation of a preshock. After a time τ has elapsed, those fluid particles having a velocity v that does not match the preshock velocity $v_{\rm s}$ may not feel much pull from the truncation waves if phase mixing is present. More precisely, resonant interactions are confined to particles such that

$$\tau\Delta v \equiv \tau|v - v_{\rm s}| \lesssim \lambda_{\rm G}. \qquad (11)$$

If τ is small, as in Figs. 1 and 3, the region of resonance will be confined to a small neighborhood of the point of resonance. In Sec. III B we shall see that around the time of appearance of a preshock the width of the associated resonance regions is typically the order of ${K_{\rm G}}^{-1/3}$. Outside of such regions, including near the preshock, the effect of truncation waves is just a small-amplitude oscillation at the Galerkin wavelength, which on Figs. 1 and 3 shows up as a thickening of the line with respect to the inviscid-limit solution.

Actually, only resonance points with positive strain produce tygers. In a region of negative strain a wave of wavenumber close to $K_{\rm G}$ will be squeezed, potentially acquiring a larger wavenumber, and thus disappearing beyond the *truncation horizon* which acts as a kind of black hole.

Observe that in the immediate neighborhood of a preshock

or of a nascent shock the strain is also negative and actually very large. Although the strongest truncation waves are generated near such points (as one would infer by a Gibbs-phenomenon argument), their growth is severely hampered by the negative strain. Hence the bulge near the preshock grows in time much more slowly than that at the positive-strain resonance point, as illustrated in Fig. 2. Actually, the effect of truncation near a shock will remain very small (and almost invisible without zooming) until the tyger has fully spread out on the ramp (cf. end of Sec. II B). This situation is in contrast with what one observes with other energy-conserving semi-discrete schemes [41], such as the dispersive one studied by Goodman and Lax [7].

B. From tygers to thermalization: the temporal evolution

It is well known that the Galerkin-truncated solution of the Burgers equation, will eventually thermalize to a Gaussian state. The simplest case is when the initial velocity v_0 integrates to zero over the spatial period. An ergodicity argument, supported by numerical simulations, suggests that the thermalized state has equipartition of energy between all Fourier modes and thus is just low-pass filtered white noise in the x variable [15, 20].

How does the highly organized and localized tyger structure seen in Figs. 1 and 3 evolve into such a totally random state?

The birth of tygers around the time $t_\star$ of the first preshock will be studied in Sec. III. In particular, in Sec. III A, we shall present evidence for scaling properties with $K_{\rm G}$ of both tyger amplitude and width at $t = t_\star$. Here we shall focus on the temporal evolution at later times. Figs. 5, corresponding to the single-mode initial condition and $K_{\rm G} = 700$, show the evolution of the tyger in terms of the discrepancy $\tilde{u} = v - u$ from $t = 1.07$ to $t = 1.50$, shortly after its birth around $t_\star = 1$. The first few panels display very symmetrical (even) bulges whose amplitudes grow in time, because truncation wave input has accumulated, while their width decreases (thinning), as a consequence of phase mixing. Rather quickly, the decrease in width leads to a collapse of the tyger, around $t = 1.19$. This is preceded and accompanied by a growing asymmetry of the tyger for which we offer the following interpretation. The tyger contains kinetic energy in the form of modulated oscillations at the Galerkin wavelength (we shall see that this increasing energy compensates the loss of energy in shocks). Over scales large compared to the Galerkin wavelength but small compared to the tyger width, this kinetic energy gives rise to an x-dependent Reynolds stress, which pulls the tyger envelope up where the envelope has a negative slope and down where the slope is positive. The resulting asymmetry becomes very conspicuous after the collapse, as seen in the last panel of Fig. 5. This panel has at least two other noteworthy features. To the right and left of the central point $x = \pi$ we see two pieces that look like a portion of ($K_{\rm G}$-truncated) white noise; this is the very beginning of thermalization. Observe that the right piece is shifted vertically with respect to the left one and that the transition looks almost like an antishock (a shock which goes up rather than down, as prescribed by the inviscid limit).

Let us also observe that around the time of collapse there is an apparent change of symmetry. Since the single-mode initial condition is odd (after shifting the origin of the x-axis to the center of the tyger) it stays odd at all later times. This is however a statement about the full solution, down to the Galerkin wavelength. If we concentrate on the larger-scale aspect (the envelope of the bulge), we find that the discrepancy is even until somewhat before collapse and odd after collapse.

For later phases of the tyger growth, it is better to show simultaneously the truncated solution and the untruncated one. Also, we switch to the three-mode initial condition which has less symmetry and is thus more generic. Fig. 6 shows the evolution from $t = 0.3$, slightly after the first singularity at $t_\star = 0.2218$, to $t = 4.5$ when the solution of the truncated problem is basically completely thermalized. From $t = 0.3$ to $t = 0.8$ we observe that the chaotic-looking thermalized regions born after collapse are growing in extent and are affecting more and more of the ramp-like structure which are a well-known feature of the solution of the untruncated Burgers equation after the formation of shocks. In short, we shall say that "the tyger spreads out on the ramp".

As long as significant tyger activity has not reached the shocks, their positions, amplitudes and motions are correctly described by the Burgers equation, down to the Galerkin wavelength. We have checked that during this phase even shock merger is unaffected by truncation (an instance is seen around $t = 1.0$). Later, strong tyger activity near the edges of shocks is able to shift them slightly (this is visible at $t = 1.3$). Once the shock amplitude has decayed to values much less than the tyger fluctuations, the solution looks globally thermalized ($t = 4.5$). It must be noted that the mechanism which prevents thermalization in the Fermi–Pasta–Ulam problem [21] does not seem to be present here.

C. 2D Euler

So far we have worked with a very special hydrodynamical equation: the Burgers equation is integrable, compressible and its solutions generically blow up after a finite time. Is the tyger phenomenon also present when none of these properties hold, as is the case for the two-dimensional incompressible Euler equation with smooth (analytic) initial data and space-periodic boundary conditions?

The short answer is "yes". We have numerically investigated quite a number of different initial conditions, including the two-mode Standard Orthogonal Case (SOC) initial condition used in [22] and random initial conditions. The simulations were done with resolutions from 512^2 to 8192^2. Here we report the results for the random initial condition, which is 2π-periodic in x_1 and x_2. The Fourier space consists of couples of signed integers $\boldsymbol{k} \equiv (k_1, k_2)$. It is here decomposed for convenience into shells corresponding to a $K \le |\boldsymbol{k}| < K+1$, where K is an integer. Each such shell has $N(K)$ Fourier modes. For $\boldsymbol{k}$ in the Kth shell, the Fourier coefficients $\hat{\omega}_{\boldsymbol{k}}$ of the initial vorticity are taken all with the same modulus $2K^{7/2}\exp(-K^2/4)/N(K)$ and with phases that

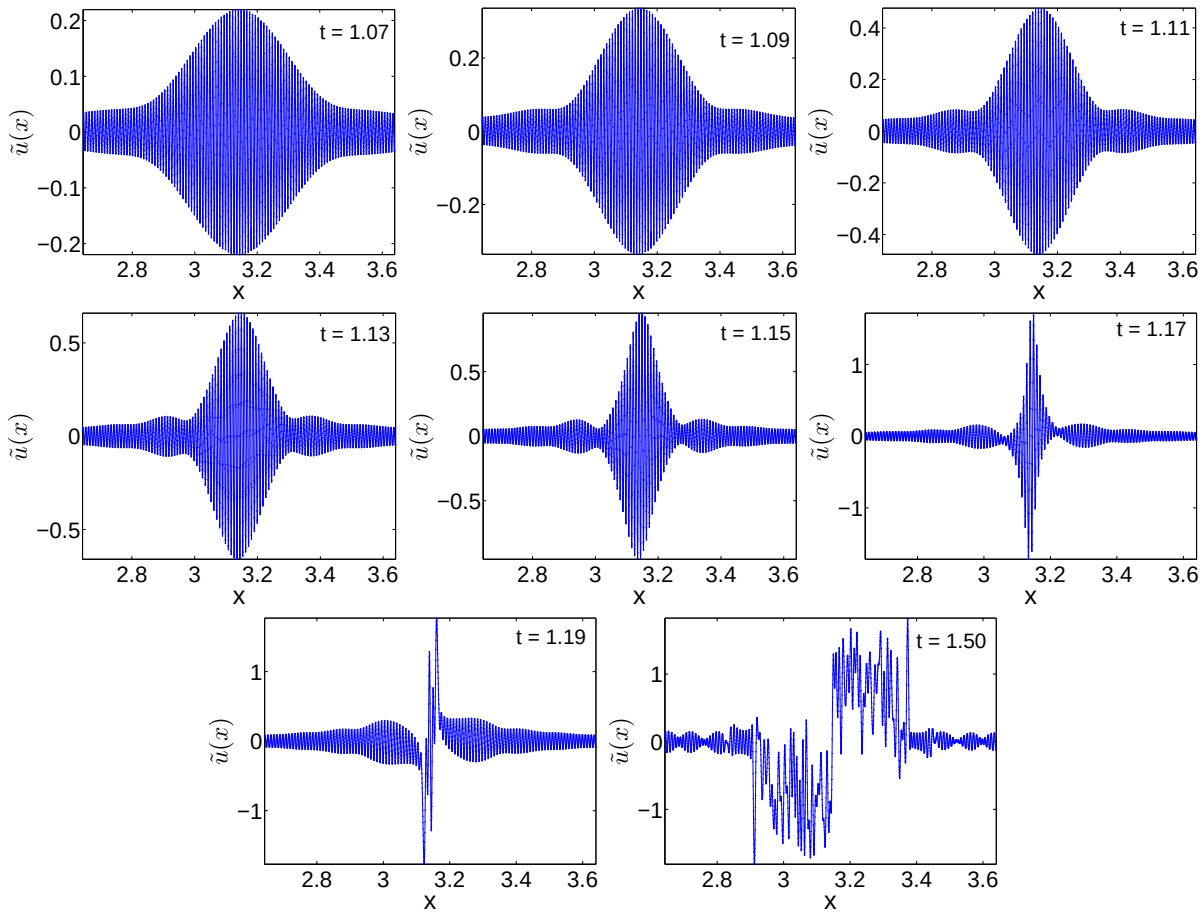

FIG. 5: (Color online) Evolution of the tyger (discrepancy) for same conditions as in Fig. 1: growth, thinning, asymmetrization, collapse and chaotization.

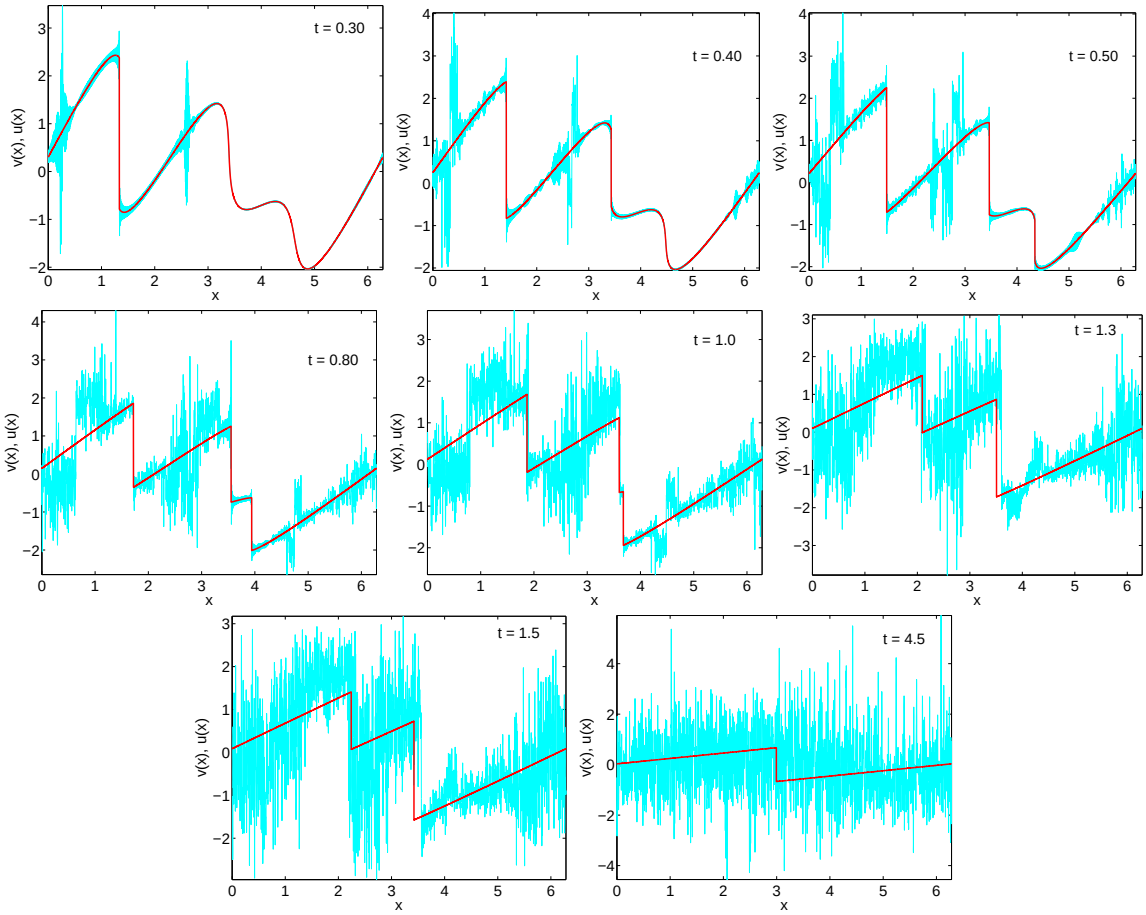

FIG. 6: (Color online) Long-time evolution of three-mode initial condition (other parameters as in Fig. 1). The cyan curve (light grey) is the Galerkin-truncated solution and the red one (black) the untruncated inviscid-limit solution. Observe that tygers progressively invade the ramps between shocks but that shocks remain sharp and correctly placed as long as the spreading out of the tygers on the ramps has not reached them. At very long times, the truncated solution is thermalized.

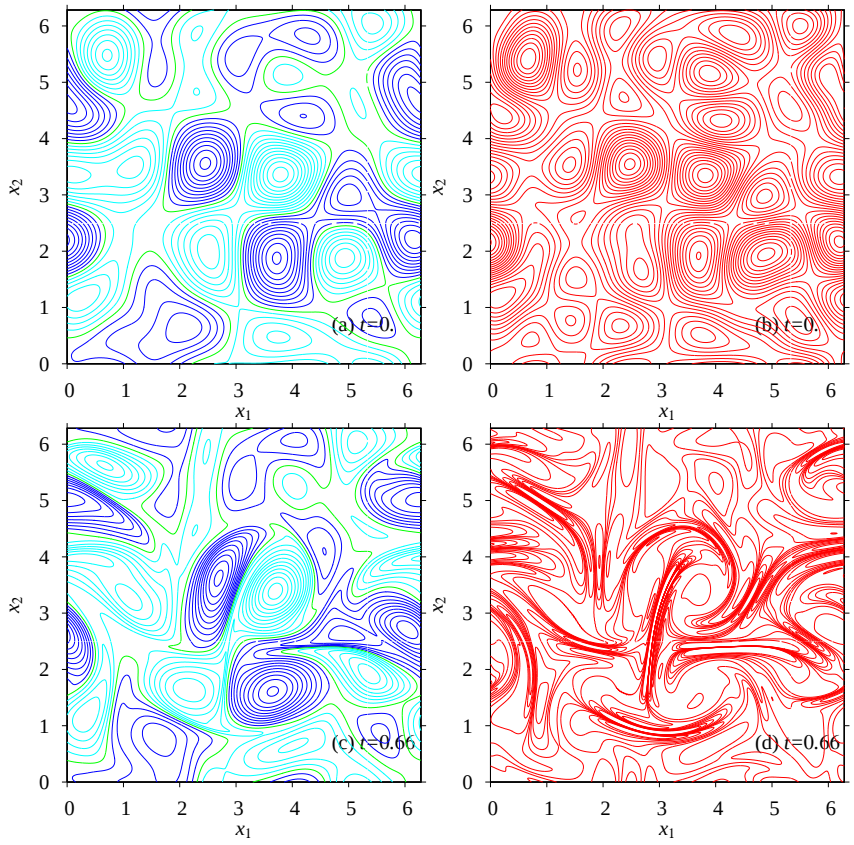

FIG. 7: (Color online) (a) shows contours of vorticity with random initial conditions; positive values in dark blue (black), negative values in light blue (light gray); (c): same at time $t = 0.66$ (before appearance of tygers); (b) and (d) are contours of the Laplacian of the vorticity at times $t = 0$ and $t = 0.66$. Notice the thin elongated red (black) "cigars" which play here the role of the preshocks/shocks in the Burgers case.

are uniformly and independently distributed in the interval $[0, 2\pi[$, except that opposite wavevectors are given opposite phases to preserve Hermitian symmetry. The tyger calculations shown here are all with resolution 1024^2 and Galerkin truncation wavenumber $K_{\rm G} = 342 = (1024 + 2)/3$. The particular realization used as initial condition in the present calculation can be retrieved from http://www.kyoryu.scphys.kyoto-u.ac.jp/~takeshi/popular.html. Fig. 7 shows the vorticity and its Laplacian at $t = 0$ and $t = 0.66$, the latest time at which no tyger is seen (at least in the fields displayed). Although for the untruncated solution real singularities are ruled out at any finite time, there is strong enhancement of spatial derivatives of the vorticity [23]. The highest values of the Laplacian is found in the straight cigar-like structure seen near the center of the figure which—as we shall see—will play an important role in tyger generation [42]. Furthermore this cigar moves very little because there is a velocity stagnation point near its center [43]. Fig. 8, which is centered on the strongest cigar, shows the development of tygers. In terms of the Laplacian of the vorticity they become visible around $t = 0.71$ and then become much stronger.

A further look at a tyger is provided in Fig. 9 which zooms into one of the tygers and also shows the Laplacian of the vorticity along a cut.

We immediately see that, as for the 1D Burgers equation, most of these tygers have come "out of the blue," namely appearing at places which had no preexisting small-scale activity; more precisely, they appear when complex-space singularities come within one Galerkin wavelength $(2\pi)/K_{\rm G}$ of the real domain. The streamlines shown in Fig. 8 indicate that tyger activity appears at places where the velocity is roughly parallel to the central cigar. As already pointed out, the cigar hardly moves; this condition is thus equivalent to having fluid particles whose distance to the cigar remains roughly constant. In so far as the cigar may be considered as a one-dimensional straight object, the truncation waves generated by the cigar will have crests parallel to the cigar and those fluid particles which move parallel to the crest keep a constant phase and thus have resonant interactions with the truncation waves. So far, this is basically the same mechanism as discussed in Sec. II A for 1D Burgers dynamics except, of course, that the flow being now incompressible, the velocity within the tyger is mostly perpendicular to the direction of fastest variation. If we now consider the one-parameter family of straight lines perpendicular to a given cigar, each such line will have some number (possibly zero) of resonance points; altogether they form the tygers. Since the flow outside cigars is fully two-dimensional, these tygers have no reason to be parallel to the cigars.

Observe that there are some points where this kind of resonance condition holds but no tyger is seen, for example in Fig. 8 at $t = 0.71$ near $x_1 = 3.8$ and $x_2 = 3.4$. This can be interpreted in terms of strain: an incompressible flow has at each point a strain matrix with two perpendicular eigendirections, one for positive strain and the other one for negative strain. Fig. 8 has little pink (light gray) segments indicating the direction of positive strain. Tyger activity is found only at resonance points where the (positive) strain direction is not far from being perpendicular to the cigar. More precisely, it is easily shown that it has to be within less than $\pi/4$ of this direction. Otherwise the near-truncation activity generated by resonance is sheared quickly beyond the truncation horizon.

It is also of interest to show truncation effects and tygers in Fourier space. Fig. 10 shows, at various times, the moduli of Fourier coefficients in the (k_1, k_2) plane on a logarithmic scale. The lowest value contours are at the 10^{-15} level, while rounding errors are about 10^{-16}. Note that the Fourier-space picture is organized in the form of one main lobe, perpendicular to the physical-space central cigar and secondary lobes associated to less intensive small-scale structures. At the earliest time $t = 0.4$ no truncation effect near $|\boldsymbol{k}| = K_{\rm G} = 342$ is visible [44]. At $t = 0.49$, long before tygers become visible on the Laplacian of the vorticity in physical space, Fourier-space truncation becomes visible. This truncation at first affects the wavevectors in the direction of the main lobe that is perpendicular to the central cigar. Truncation effects then spread progressively to other angular directions but appear to do so continuously, in contrast to physical space where tygers are born "out of the blue." We can actually see such early truncation effects in physical space by taking more spatial derivatives and thus putting more weight on high wavenumbers. At $t = 0.49$, Fig. 11 shows contours of the tri-Laplacian $(\nabla^2)^3\omega$ with wiggly tygers. By performing various cuts (not shown), we checked that the spatial variation is mostly perpendicular to the cigar.

Recently we checked that many features observed for 2D incompressible Euler tygers are also present in the 3D case. The details will be reported elsewhere.

D. The dissipative anomaly and the lack of weak limit

Earlier in this paper, we have seen that for large values of the truncation wavenumber $K_{\rm G}$, the Galerkin-truncated solution remarkably preserves many features of the inviscid limit such as shocks and their dynamics. So we ask: could it be that the Galerkin-truncated Burgers equation converges in a suitable sense to the inviscid limit solution as $K_{\rm G} \to \infty$? This question was actually the main motivation of the present work. We shall see that the answer is "no", but a qualified no.

First, for the kind of analytic initial conditions considered here that go singular at some finite time $t_\star$, the answer to the above questions is actually "yes" for times $0 \le t < t_\star$. At such times, the solution of the Burgers equation in Fourier space for large wavenumbers is bounded by $Ce^{-\delta k}$ (see Appendix B). The effect of truncation is thus exponentially small in $K_{\rm G}$ and should go away when $K_{\rm G} \to \infty$. For the two-dimensional incompressible Euler equation with periodic analytic initial data, analyticity holds for arbitrary large times and thus the Galerkin-truncated solution is expected to converge to the untruncated solution [45]. For three-dimensional flow the situation may depend on whether or not there is finite-time blow up, a question which is very much open (cf. [10, 11] and references therein.)

Returning to the one-dimensional Burgers case, what about

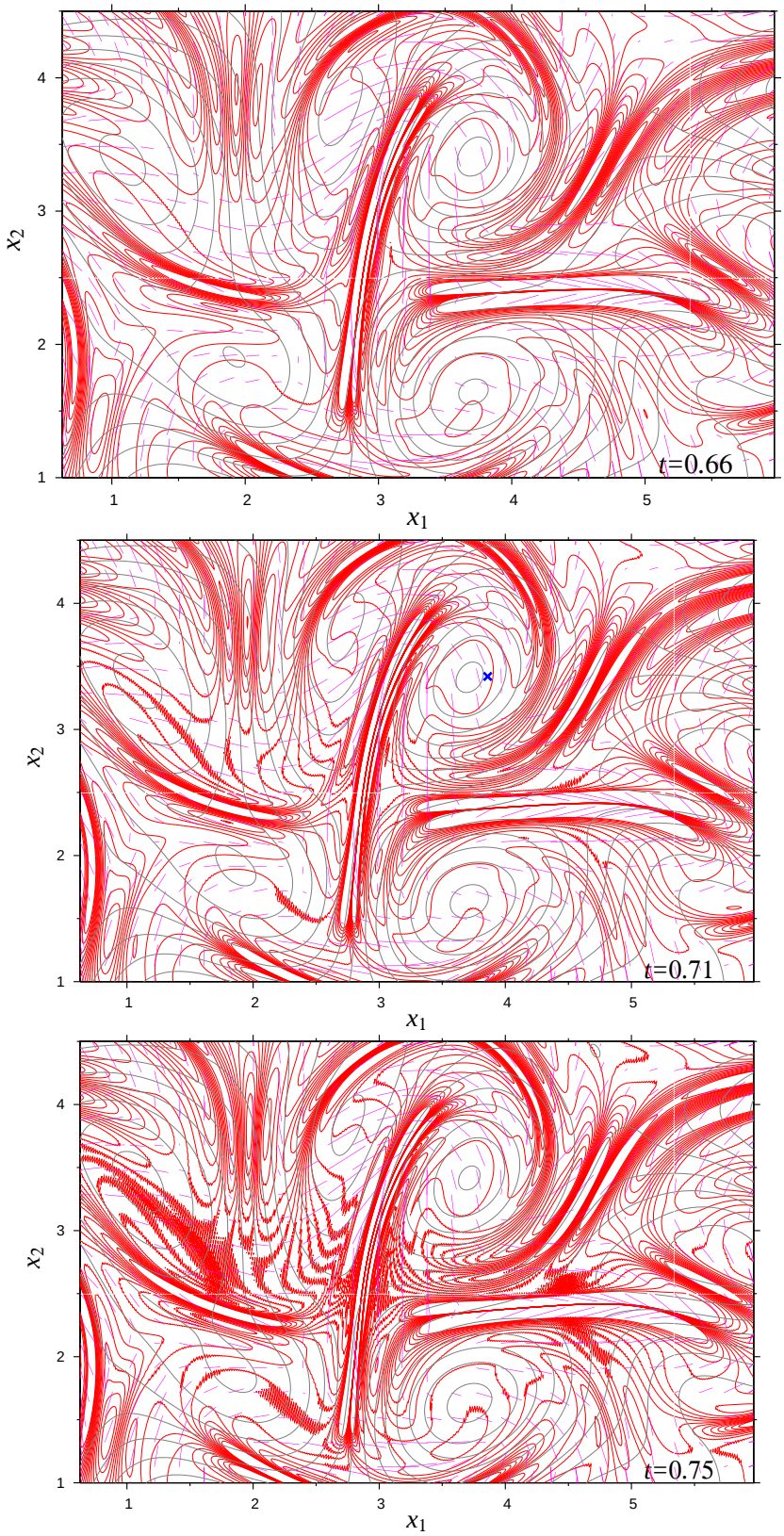

FIG. 8: (Color online) A 2D tyger: before ($t = 0.66$), early ($t = 0.71$) and later ($t = 0.75$). Figures, moderately zoomed, centered on the main cigar. Contours of the Laplacian of vorticity in red (black), ranging from -200 to 200 by increments of 25, streamlines in gray, ranging from -1.6 to 1.6 by increments of 2 and positive strain eigendirections in pink (light gray) segments. Notice tygers appearing at $t = 0.71$ in the form of wavy red (black) contours at places where the velocity is roughly parallel to the main cigar; later, the tygers grow in strength and extension. A blue (black) x-mark is added at $t = 0.71$ to underline that there is no tyger, in spite of resonance, because of a wrong strain direction.

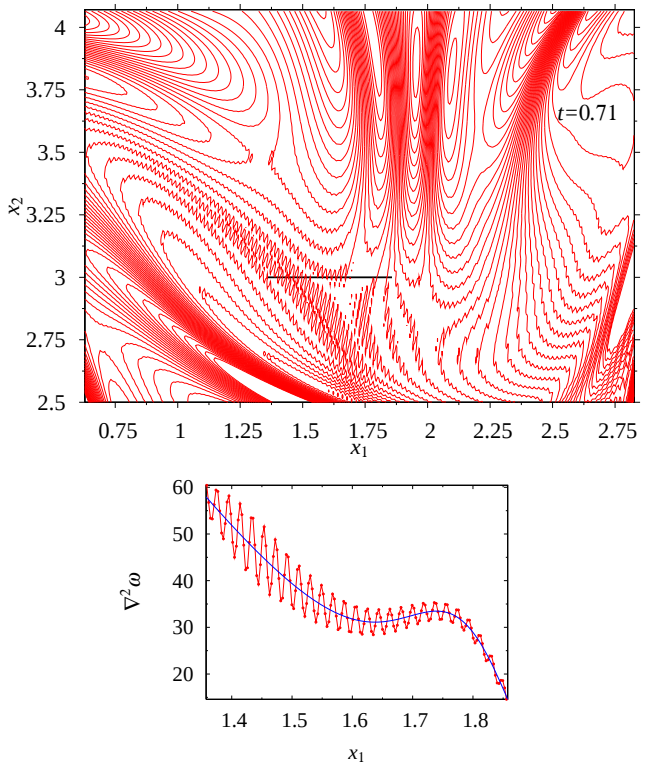

FIG. 9: (Color online) Upper: zoomed version of contours of the Laplacian of vorticity at $t = 0.71$. Lower: plot of the Laplacian of vorticity along the horizontal segment near $x_2 = 3$, shown in the upper panel.

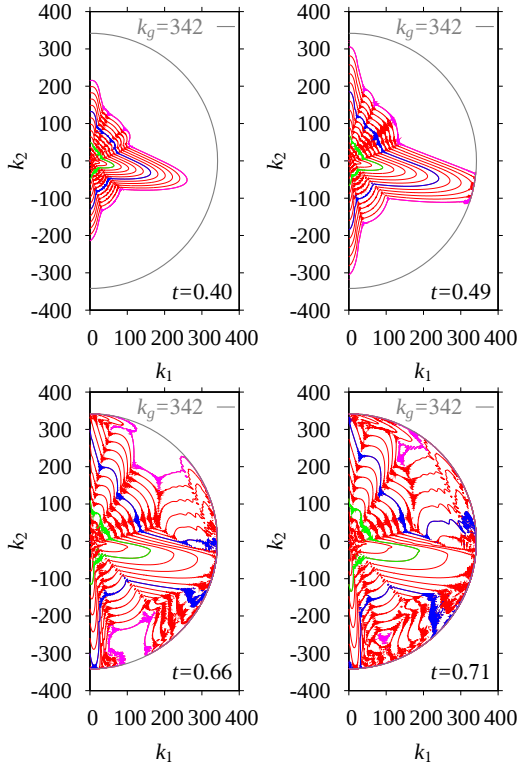

FIG. 10: (Color online) Contours of the modulus of the vorticity Fourier coefficients at various times. Negative k_1 values not shown because of Hermitian symmetry. Contour values are 10^{-1}, $10^{-2}, \ldots, 10^{-15}$ from inner to outer (in color version, green, blue and pink highlight the values $10^{-5}, 10^{-10}$, and 10^{-15}, respectively). Galerkin truncation effects are visible above the rounding level already at $t = 0.49$ and become more and more invasive.

$t > t_\star$, when shocks are present and the solution is *dissipative*, whereas the Galerkin-truncated solution is *conservative*? How can such a conservative system mimic the dissipative anomaly? One could imagine that the small-scale tyger activity plays the role of molecular motion and that motion on scales much larger than the Galerkin wavelength is governed by the inviscid-limit Burgers equation.

This is however not the case. Tadmor investigated the limit—in a suitable sense to be defined below—of the truncated solution and found that it cannot be dissipative (Ref. [18] p. 31). The limit considered by Tadmor and in other papers studying conservative modifications of the Burgers equation with strong oscillations [6–8] is a distributional *weak* limit. Assuming that the Galerkin-truncated solution v has a weak limit $\overline{v}$ satisfying the Burgers equation, and using the basic dynamical equations (4)-(5), Tadmor shows that v^2 has the weak limit $(\overline{v})^2$, from which he infers that the limit is actually a strong one which implies energy conservation and contradicts the dissipative character of the solution to the Burgers equation. Recently numerical simulations of the inviscid Galerkin-truncated Burgers equation with $K_{\rm G}$ up to about 10^4 showed indeed that such solutions do not converge to the inviscid limit of the untruncated solution [25].

The simplest instance of such a weak limit is just to apply a low-pass filter to the solution with a fixed threshold K for the modulus of the wavenumber, while letting $K_{\rm G} \to \infty$. It is

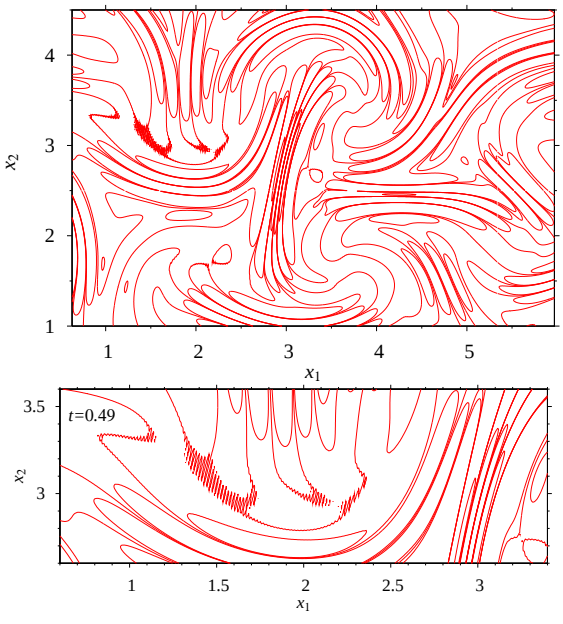

FIG. 11: (Color online) Contours of tri-Laplacian of the vorticity (upper: zoomed; lower: superzoomed) showing a tyger already at $t = 0.49$.

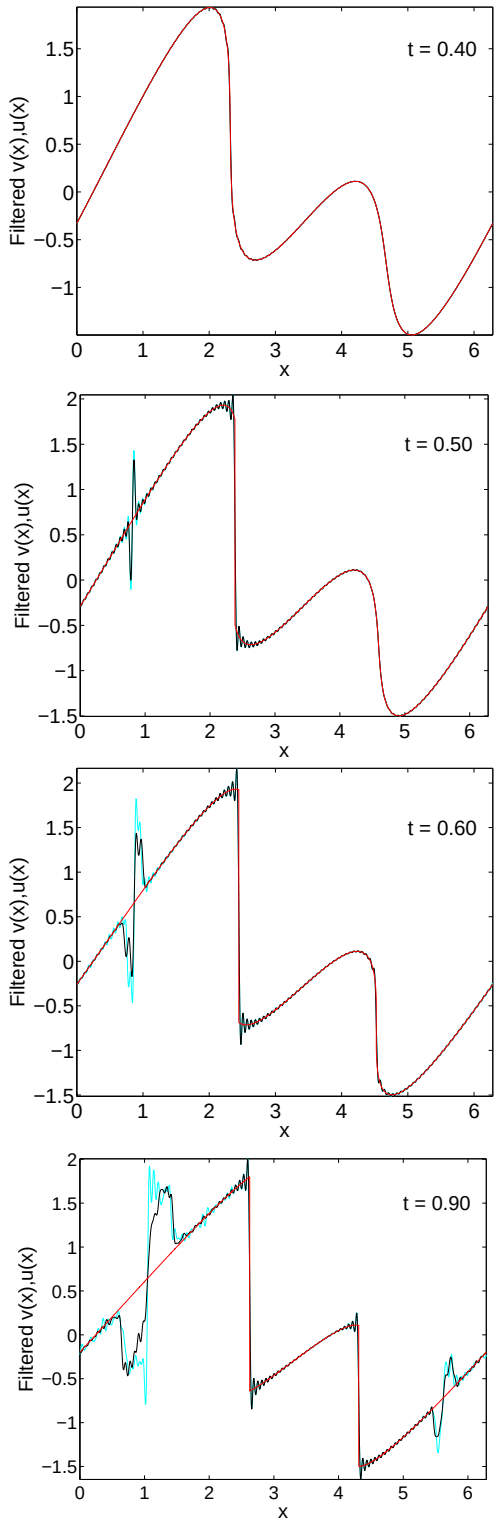

FIG. 12: (Color online) Plots of solution of the Galerkin-truncated Burgers equation, with $K_G = 5,461$ in cyan (light grey) and $K_G = 21,845$ in black, low-pass filtered at wavenumber $K = 100$, at various times. Initial condition $v_0(x) = \sin(x)+\sin(2x-0.741)$. The untruncated solution is shown in red (black, mostly straight line).

then easy to show that one can find a subsequence $n_1, n_2, \ldots$ of the sequence of integers $K_{\rm G}$ such that the low-pass filtered solution has a limit [26]. We have obtained evidence that, without taking subsequences, there is no weak limit. Indeed Fig. 12 shows the low-passed solution with the same threshold $K = 100$ for the same initial condition and the same output time, but for two very large and well-separated values of the truncation: $K_{\rm G} = 5,461$ (denoted 5K) and $K_{\rm G} = 21,845$ (denoted 21K). The solutions agree very well with the untruncated solution at shocks and nearby but the 5K and 21K tygers differ significantly, even after application of the low-pass filter. It may thus be that there is no weak limit as $K_{\rm G} \to \infty$ [46].

We can supplement this by a more physical and fluid mechanical explanation of why the truncated solution cannot converge (weakly) to the inviscid-limit solution. We have seen in Sec. II B that shocks behave just as predicted by the inviscid limit for a substantial length of time (until tyger spreading on the ramp reaches the shocks). Because of this, the hypothetical limit of the truncated solution would be losing energy at the shocks, just as the ordinary Burgers equation. The energy lost has to be found in the tygers in the form of high-wavenumber oscillations. Decomposing the truncated solution $v = u + \tilde{u}$ (where u is the inviscid-limit solution) we obtain tyger Reynolds stresses $\overline{\tilde{u}^2/2}$, where the overline means a *mesoscopic* spatial averaging over a distance large compared to the Galerkin wavelength and small compared to any macroscopic scale (for example using a low pass filter with threshold $K = 100$ for the case $K_{\rm G} = 5,461$). If the mesoscopic tyger energy and thus the Reynolds stress is not spatially uniform, its gradient will drive the flow away from the inviscid limit. This is the same mechanism that makes the tyger asymmetrical, as already mentioned. Is there a way to obtain the correct inviscid limit by eliminating the undesirable Reynolds stresses through some kind of *tyger purging*? We shall come back to this important practical issue in the last section.

Finally, let us remark on our choice of the word *tyger* for the oscillations which are a result of Galerkin truncation. Historically, the distinction between conservative and dissipative systems has played a crucial role in not only man's scientific pursuits, but also in a deeper cultural context. For centuries there was a certain sanctity associated with things conservative as opposed to being dissipative. Hence, before Galileo's telescope revealed the "transient" nature of celestial occurrences (e.g., Sun spots), man had always ascribed heavenly objects as conservative and the more mundane, transient, and earthly occurrences as dissipative. The fine balance of the two seemed essential for all existence.

In the backdrop of this and in our investigations of truncated systems, William Blake's poem "The Tyger" assumes special significance `http://en.wikipedia.org/wiki/The_Tyger`. In most interpretations, Blake's tyger is of course not the animal itself [47]; it is a metaphor for the symmetry of seemingly different, even opposite, processes which nonetheless combine to make a coherent whole. Thus apparent oppositions such as life and death, light and darkness are seamlessly unified. In our present study, we explore the

interplay of conservative and dissipative dynamics: how one, surprisingly, might be embedded into another. As a result, it was quite natural for us to call this phenomenon a tyger.

III. DETAILED ANALYSIS OF THE BIRTH OF THE BURGERS TYGER

So far our point of view has been that of the (numerical) experimentalist, with some amount of phenomenological theory used to interpret the results whenever possible. In this section we shall use a lot more "systematic theory", namely expansions for large values of the Galerkin truncation wavenumber $K_{\rm G}$. In principle, such expansions can be carried out beyond leading order; we shall however not attempt this, let alone obtain rigorous bounds for errors. Indeed some of our approximations used below are akin to what one calls "patching" (as opposed to "matching") in boundary layer theory, that is approximations which can give the correct exponent of a power-law leading term but cannot predict the correct constant in front.

Let us now give a general overview of how we intend to proceed. We shall concentrate on a single problem, that of the birth of the tyger for the one-dimensional Burgers equation with single-mode initial condition. The birth, which takes place around the "Galerkin time" $t_{\rm G}$ when complex singularities come within one Galerkin wavelength from the real domain, is part of an early phase which extends from $t = 0$ to the time of the first singularity $t = t_\star = 1$. In Sec. III A we shall see that the early tyger at $t = t_\star$ has remarkable scaling properties with $K_{\rm G}$. Our intention here is to understand analytically how this comes about. For this, our strategy will be to devise various models/approximations which make the problem simpler while hopefully keeping the leading-order behavior unaffected. There will be three levels of modelling: (i) linearization around the untruncated solution, (ii) ignoring the "exponentially small" phase up to the Galerkin time $t_{\rm G}$, and (iii) "freezing", i.e. replacing the untruncated solution $u(x,t)$ by $u_\star(x) \equiv u(x,t_\star)$ for $t \in [t_{\rm G}, t_\star]$. In Sec. III B we explain how to do this and why it is justified. The problem is then reduced to studying a linear first-order differential equation with constant coefficients in a finite dimensional space (Sec. III C). It was brought to our attention recently by J. Goodman that this differential equation has features in common with that studied by Goodman, Hou and Tadmor (subsequently cited as GHT) in connection with the stability of the pseudospectral method in the presence of aliasing [28].

A. Scaling properties of the early tyger

In Sec. II we have seen that tygers are born at suitable resonance points in the form of bulges made of oscillation at the Galerkin wavelength with a very symmetrical envelope. Eventually, Reynolds stresses will distort this envelope. At the time $t_\star$ of the first singularity this is not yet the case. Now we concentrate on the scaling properties for high $K_{\rm G}$ of the amplitude a and width w of such early tygers, in terms of the discrepancy $\tilde{u} = v - u$. Here we limit ourselves to the single-mode initial condition. Figs. 13 and 14 show respectively the amplitude and width as a function of $K_{\rm G}$ for values ranging from 100 to 40,000. The amplitude is measured at the maximum closest to the center of the tyger, located a distance $\pi/(2K_{\rm G})$ away. The width is measured at half of this amplitude. It is seen that both have clean scaling laws for sufficiently large $K_{\rm G}$: subdominant corrections are perceptible on the log-log plots only for $K_{\rm G} < 200$. The leading-order behavior is

$$a \propto {K_{\rm G}}^{-2/3}, \qquad w \propto {K_{\rm G}}^{-1/3}. \tag{12}$$

The following sections are mostly devoted to explaining these scaling laws.

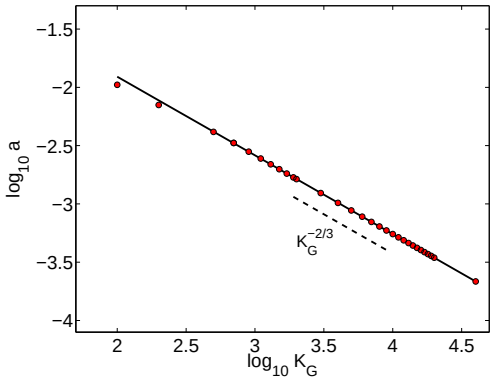

FIG. 13: (Color online) A log-log plot of the discrepancy-based amplitude a of the tyger at time $t = t_\star$ as a function of $K_{\rm G}$. Initial condition $u_0(x) = \sin x$. The data points are shown by filled red circles (black circles) and the thick black line is the best power-law fit $\propto K_G^{-2/3}$, which holds over two decades.

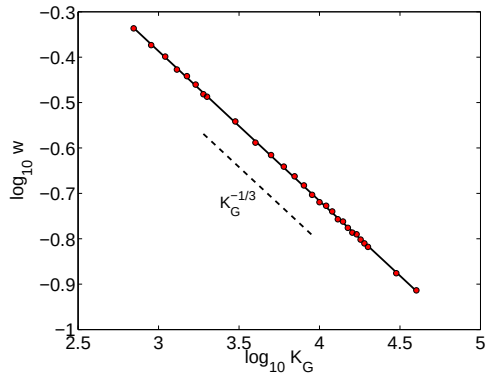

FIG. 14: (Color online) Log-log plot of the width (at half amplitude) of the tyger. Otherwise, same as in Fig. 13. The best power-law fit is now $\propto K_G^{-1/3}$, which holds over nearly two decades.

B. Three successive approximations

As already observed in Sec. II D, initial conditions with a finite number of Fourier harmonics, such as the single-mode

case, are for a while analytic in the complexified space variable within a strip around the real domain of width $\delta(t)$. As long as $\delta(t)K_{\rm G} \gg 1$ the effect of truncation is exponentially small. This is why, the kind of tygers reported in Sec. II are not seen before $t_{\rm G}$, when complex singularities come within roughly one Galerkin wavelength from the real domain. For large $K_{\rm G}$, this happens only a short time $O({K_{\rm G}}^{-2/3})$ before the time $t_\star$ of the first singularity (cf. Appendix B). Hence, by the time $t_\star$, truncation has been felt significantly only for a lapse of time $O({K_{\rm G}}^{-2/3})$. The phase mixing argument given in Sec. II A and in particular (11) tell us that the coherent build up of a tyger will affect only those locations whose velocity differs from that at resonance by an amount Δv such that

$$\Delta v \lesssim \frac{2\pi}{{K_{\rm G}}^{-2/3}K_{\rm G}} \propto {K_{\rm G}}^{-1/3}. \tag{13}$$

Since at such times, the velocity v of the truncated solution is expected to stay close to the velocity u of the untruncated solution and the latter varies linearly with x near the resonance point, the width of the $t_\star$ tyger is itself proportional to ${K_{\rm G}}^{-1/3}$, as indicated by the simulations.

Is there an equally simple argument to understand why the amplitude scales as ${K_{\rm G}}^{-2/3}$? One possibility would be to observe that at $t_\star$ the untruncated solution has a cubic root behavior near the preshock location (cf. Appendix B). If we cut out a small interval of length one Galerkin wavelength $\lambda_{\rm G}$, we will be "missing" an energy $\sim \int_0^{\lambda_{\rm G}} x^{2/3}dx \sim {K_{\rm G}}^{-5/3}$. Remembering that the Galerkin-truncated equation conserves energy, if we assume that this missing energy is transferred entirely to a tyger of width ${K_{\rm G}}^{-1/3}$, we obtain precisely an amplitude $\propto {K_{\rm G}}^{-2/3}$. There is however no reason to assume that near the preshock the effect of truncation can be reduced to carving out a little interval of one Galerkin wavelength. It is doubtful that this energy argument can be turned into something rigorous.

We turn now to more systematic arguments. Before $t_\star$, when $\delta(t) > 0$, it is easily shown that the Galerkin-truncated solution converges strongly to the untruncated solution. The simulations reported in Sec. III A suggest that this still holds at $t = t_\star$, since the amplitude of the discrepancy goes to zero. Furthermore, the nonlinear effect of Reynolds stresses, as discussed in Sec. II D is of even higher order. Indeed, within the bulge the Reynolds stresses will be $\sim {K_{\rm G}}^{-4/3}$; since they change spatially on a scale $\sim {K_{\rm G}}^{-1/3}$, the gradient of Reynolds stresses is $\sim {K_{\rm G}}^{-1}$; over a time interval $\sim {K_{\rm G}}^{-2/3}$ this will change the bulge amplitude by $\sim {K_{\rm G}}^{-5/3}$, which is small compared to the amplitude of the bulge itself.

All this suggests that the early tyger development can be captured by somehow linearizing the Galerkin truncated solution around the untruncated one. Let us rewrite the basic dynamical equations (4)-(5) in terms of the discrepancy

$$\tilde{u} \equiv v - u. \tag{14}$$

We obtain

$$\partial_t \tilde{u} + {\rm P}_{K_{\rm G}}\partial_x\left(u\tilde{u} + \frac{\tilde{u}^2}{2}\right) = \left({\rm I} - {\rm P}_{K_{\rm G}}\right)\partial_x\frac{u^2}{2}, \quad \tilde{u}(0) = 0, \tag{15}$$

where I stands for the identity operator and the zero initial condition follows from $u_0 = v_0$, a consequence of having a finite number of modes initially.

Observe that the r.h.s. of (15) provides no input to wavenumber below the truncation. Actually this input is hidden in the l.h.s. To make this clear, we need to decompose the various fields into their Galerkin-truncated part and the remainder. We set

$$u = u^< + u^> \tag{16}$$

$$u^< \equiv {\rm P}_{K_{\rm G}}u \qquad u^> \equiv ({\rm I} - {\rm P}_{K_{\rm G}})u. \tag{17}$$

Next, to similarly decompose $\tilde{u}$, we use $({\rm I} - {\rm P}_{K_{\rm G}})\tilde{u} = -u^>$, which follows from the fact that $v = u + \tilde{u}$ has no harmonics beyond the truncation. Hence we have

$$\tilde{u} = u' - u^>, \tag{18}$$

$$u' \equiv {\rm P}_{K_{\rm G}}\tilde{u}. \tag{19}$$

In what follows we shall work mostly with u' which has no harmonics beyond the truncation and which we call the *perturbation*. As we shall see, around $t_\star$, the perturbation is small. In contrast, beyond the truncation, the discrepancy is just equal to minus the untruncated flow; it is thus known but in no way small. Now, we apply ${\rm P}_{K_{\rm G}}$ to (15) and use the various decompositions to obtain

$$\partial_t u' + {\rm P}_{K_{\rm G}}\partial_x\left(uu' + \frac{(u')^2}{2}\right) = {\rm P}_{K_{\rm G}}\partial_x\left(u^< u^> + \frac{(u^>)^2}{2}\right). \tag{20}$$

The r.h.s. of (20) is a known function which we shall call the *beating input* and denote f because it describes how harmonics of the untruncated solution, located beyond the truncation, interact with themselves or with subtruncation harmonics to give a subtruncation input. This beating input, which is shown in the lower panel of Fig. 19, consists basically of spatial oscillations at the Galerkin wavelength, modulated by an envelope that peaks at the preshock. This is the precise content of what we called "truncation waves" in the phenomenological approach of Sec. II A

We are now in a position to define the three approximations made for large $K_{\rm G}$, which we call respectively *linearization*, *reinitialisation* and *freezing*:

- 1. The term $(u')^2$ in the l.h.s. of (20) is discarded;
- 2. The perturbation u' is set to zero at time $t_{\rm G}$;
- 3. The untruncated solution is frozen to its $t_\star$ value.

Concerning linearization, we already observed that nonlinear effects will be weak if the scaling laws for the $t_\star$ tyger are indeed given by (12). Reinitialization is justified because, prior to the Galerkin time $t_{\rm G}$, only exponentially small perturbation are present and, here, we are only trying to capture algebraically small terms. It is then convenient to introduce a new shifted time variable

$$\tau \equiv t - t_{\rm G}. \tag{21}$$

To avoid unnecessary constants, we choose, $t_{\rm G} = t_\star - {K_{\rm G}}^{-2/3}$. Hence, in the τ variable, the first real (preshock) singularity is at

$$\tau_\star \equiv {K_{\rm G}}^{-2/3}. \tag{22}$$

We shall also take the liberty to still denote the perturbation by u' when it is expressed in terms of the shifted time. As to the freezing, replacing $u(t)$ by $u_\star \equiv u(t_\star)$, it appears justified since the untruncated solution hardly changes between $t_{\rm G}$ and $t_\star$, except at wavenumbers much larger than $K_{\rm G}$ which do not contribute to (20). Freezing changes (20) into an equation with constant coefficients. In particular the beating input becomes time-independent.

Although there are good theoretical reasons to make these three approximations, we also tested them numerically. Fig. 15 shows the scaling law for the tyger amplitude at $t_\star$ in compensated form (after multiplication by ${K_{\rm G}}^{+2/3}$) for (i) the full problem, (ii) with only linearization assumed and (iii) with in addition reinitialization and freezing assumed. All three cases have the same scaling law. Linearization brings about only a minuscule change, as expected. The other two approximations make a difference of about twenty percent, an indication that they can be refined.

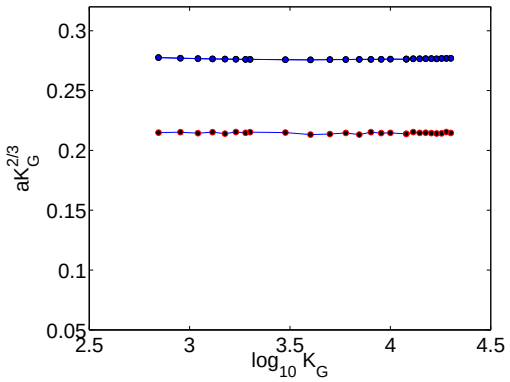

FIG. 15: (Color online) Log-linear plot of the compensated amplitude of the tyger $K_G^{2/3}\, a(K_{\rm G})$, calculated (i) from $\tilde{u}$, (ii) from the linearised approximation for u', and (iii) from the freezing plus reinitialization approximation, all versus $K_{\rm G}$. The data corresponding to (i) and (ii) are indistinguishable and shown as blue filled circles (black upper curve). The data corresponding to (iii), shown by black filled circles with a red border (black lower curve), have the same scaling but a multiplicative constant about twenty per cent lower.

C. Tyger birth: the minimal model

With all three approximations formulated in the previous section, the temporal dynamics of the perturbation near $t_\star$ is simply given by

$$\frac{d}{d\tau}u' = Au' + f, \qquad u'(0) = 0, \tag{23}$$

$$A \equiv -{\rm P}_{K_{\rm G}}\partial_x\,(u_\star\,\bullet)\,, \tag{24}$$

$$f \equiv {\rm P}_{K_{\rm G}}\partial_x\left(u_\star^< u_\star^> + \frac{(u_\star^>)^2}{2}\right). \tag{25}$$

It is important to stress that, because of the freezing approximation, A and f are evaluated at $t_\star$ and thus time-independent.

We shall now write this equation as a finite-dimensional linear differential equation by working in Fourier space and see that A is actually a matrix. Some of the quantities that we shall look at are more conveniently represented by taking the initial condition $u_0 = \sin x$, which has the tyger born near $x = 0$ and the preshock at $x = \pi$. For other quantities the choice $u_0 = -\sin x$ is better. We shall refer to the former as "origin at the tyger" and to the latter as "origin at the preshock". Note that in both cases, the initial condition being real and odd, so are the untruncated solution u, the truncated one v, the perturbation u' and the beating input f. Hence their Fourier coefficients $\hat{u}_k$, $\hat{v}_k$, $\hat{u}'_k$ and $\hat{f}_k$ are pure imaginary and odd functions of k. With this notation, it is easy to rewrite (23)-(25) as a system of $2K_{\rm G}+1$ equations, indexed by $k \in [-K_{\rm G},\, K_{\rm G}]$:

$$\frac{d}{d\tau}\hat{u}'_k = \sum_{k'=-K_{\rm G}}^{K_{\rm G}} A_{kk'}\,\hat{u}'_{k'} + \hat{f}_k\,, \qquad \hat{u}'_k(0) = 0, \tag{26}$$

$$A_{kk'} \equiv -{\rm i}k\,\hat{u}_{\star,\,k-k'}\,, \tag{27}$$

$$\hat{f}_k \equiv {\rm i}k \sum_{p+q=k} (\hat{u}^<_{\star p}\,\hat{u}^>_{\star q} + \frac{1}{2}\hat{u}^>_{\star p}\,\hat{u}^>_{\star q}). \tag{28}$$

It is important to observe that, $\hat{u}^<_{\star,\,k-k'}$ being pure imaginary, the entries of the matrix A are all real.

Here we observe that GHT were led, at the technical level, to studying a *homogeneous* version of (26) without the beating input f (and thus without resonant wave interactions). In their work, the velocity u is also prescribed but mostly taken to be $\sin(x)$ or $\sin(px)$. The operator/matrix $A_{kk'}$ differs only marginally from ours, due to the deliberate presence of aliasing.

It is of course quite easy to solve (26)-(28) numerically for the perturbation $\hat{u}'(\tau_\star)$. Fig. 16 shows its imaginary part for three large values of $K_{\rm G}$. Most of the activity is concentrated in boundary layers near $\pm K_{\rm G}$ (we are only showing the right boundary layer because the function is odd). In the "tail" outside of this boundary layer the amplitude of the perturbation is very small. The Fourier space boundary layer contains all the information about spatial oscillations on scales close to the Galerkin wavelength. If a tyger is localized in physical space near X, the Fourier amplitude will have a phase factor ${\rm e}^{-{\rm i}kX}$. For this particular set of figures we have taken the origin at the preshock. In the boundary layer the most conspicuous features are even-odd oscillations which are a signature of a tyger located at $X = \pi$. The oscillations are not completely symmetrical between positive and negative values, an

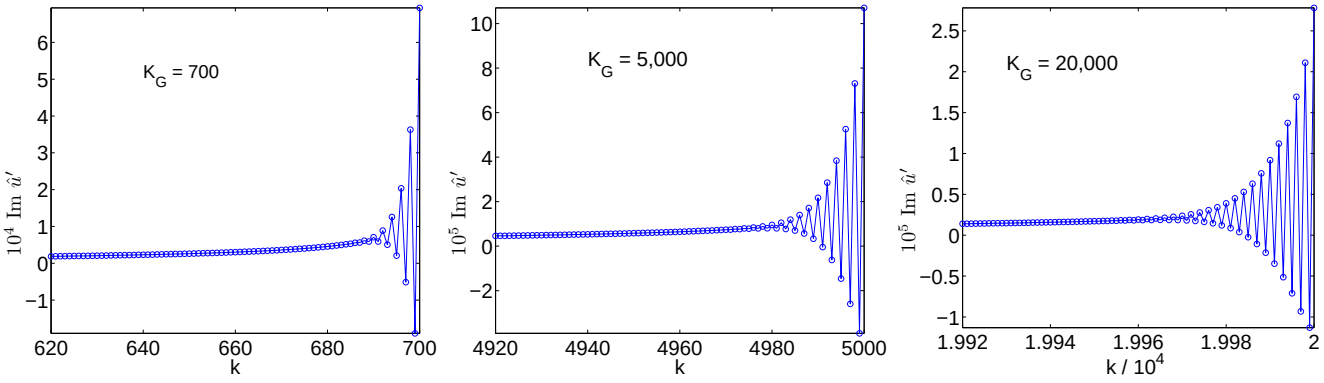

FIG. 16: (Color online) The boundary layer in Fourier space near $K_{\rm G}$. Shown are the imaginary parts of $\hat{u}'(t_\star)$ for three values of $K_{\rm G}$. The origin is at the preshock. The even-odd oscillations indicate that most of the activity is at the tyger, a distance π away.

indication that there is also some small-scale activity near the preshock at $X = 0$. The low-amplitude tail to the left of the boundary layer has no oscillations, indicating that it comes mostly from the neighborhood of the preshock. The width of the boundary layer is found to scale approximately as ${K_{\rm G}}^{1/3}$, that is the inverse of the tyger width, as expected from Heisenberg's "uncertainty principle" [48]. As to the peak amplitude of the perturbation in the boundary layer, it is found to scale as ${K_{\rm G}}^{-1}$. After subtraction of the high-k contribution stemming from the neighborhood of the preshock [49], we found that the upper part of the envelope of the boundary layer has the following scaling representation:

$$\mathrm{Im}\,\hat{u}'_k = {K_{\rm G}}^{-1} F\left(\frac{K_{\rm G}-k}{{K_{\rm G}}^{1/3}}\right), \qquad F(x) = 0.448\,\mathrm{e}^{-3.45x}, \tag{29}$$

which implies a collapse of all the boundary layer data after suitable rescaling, as illustrated in Fig. 17.

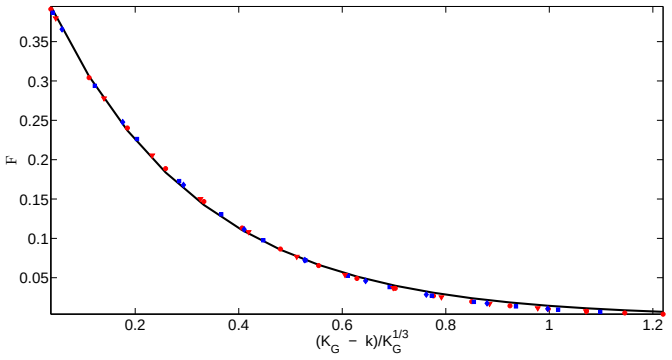

FIG. 17: (Color online) The envelopes of the various boundary layers shown in Fig. 16 (with preshock contributions subtracted out), collapsed into a single curve after rescaling. Red (black) circles: $K_{\rm G} = 20,000$, blue (black) squares: $K_{\rm G} = 15,000$, red (black) triangles: $K_{\rm G} = 10,000$, blue (black) diamonds: $K_{\rm G} = 5,000$. The thick black line is the exponential fit (29).

Note that by Fourier transformation, (29) immediately implies the basic scaling laws (12) for the width and amplitude of the tyger. As we have seen, the ${K_{\rm G}}^{-1/3}$ dependence of the width is just a consequence of the phase mixing condition (11). In the next section we shall try to understand how the amplitude factor comes about.

D. Tyger birth reduced to a simple (?) linear algebra problem

Obviously, (23) can be solved for the perturbation at time $\tau_\star = t_\star - t_{\rm G}$:

$$u'(\tau_\star) = A^{-1}\left(\mathrm{e}^{\tau_\star A} - \mathrm{I}\right) f = \left(\sum_{n=0}^{\infty} A^n \frac{\tau_\star^{n+1}}{(n+1)!}\right) f. \tag{30}$$

If the matrix A is singular (as it actually is), the middle equation of (30) is not directly meaningful, but the r.h.s. remains meaningful.

From this it becomes clear that much is controlled by the *spectral* properties of the operator A. We are thus led to consider the associated eigenvalue/eigenvector equation

$$A\psi = \lambda\psi, \tag{31}$$

which plays for the Galerkin-truncated problem the role of the standard Orr-Sommerfeld equation [29] and will be thus called. Detailed spectral properties of the Orr–Sommerfeld operator A, which is neither Hermitian nor antihermitian, are discussed in Appendix D. The eigenvalues, most of which are complex, come in opposite pairs; the associated complex eigenvectors being either even or odd functions of k. In addition there is a zero mode, i.e. an eigenvector with eigenvalue zero. We denote the eigenvalues by λ_j where j is a signed integer varying from $-K_{\rm G}$ to $K_{\rm G}$. For positive j, λ_j is the jth eigenvalue with positive imaginary part, eigenvalues being ordered by increasing moduli; $\lambda_{-j} = -\lambda_j$ and $\lambda_0 = 0$. A complete set of complex eigenmodes is denoted $\psi^{(j)}$ and their Fourier coefficients by $\psi_k^{(j)}$. When $K_{\rm G}$ is large, the eigenvalues with large indices j are almost pure imaginary and the largest (in moduli) eigenvalues are very close to $\pm\mathrm{i}K_{\rm G}$ [50]. The typical spacing between the moduli of successive eigenvalues is order unity for large $K_{\rm G}$.

Also of importance are the strength and scaling properties of the beating input, which are discussed in Appendix C. Its Fourier coefficients $\hat{f}_k$ are pure imaginary and odd functions of k. We saw that the tyger has the unexpected feature that it appears away from the preshock. However the beating input, which is caused directly by truncation, is mostly localized where the untruncated solution displays its highest small-scale activity, namely near the preshock. With the origin taken at the preshock, the imaginary part of the beating input $\mathrm{Im}\,\hat{f}_k$ peaks at truncation $k = K_{\mathrm{G}}$ with $|\hat{f}_{K_{\mathrm{G}}}| = O\left({K_{\mathrm{G}}}^{-1/3}\right)$. When moving down from K_{G} to lower k, it falls off rather slowly as $(K_{\mathrm{G}} - k)^{-1/3}$ while keeping a constant sign. Thus in Fourier space we have a rather broadband beating input. In the physical space the beating input is mostly an oscillation at the Galerkin wavelength, whose envelope falls off as $|x|^{-2/3}$, where $|x|$ is the distance from the preshock location.

Let us now decompose the beating input f and the solution $u'(\tau_\star)$ in terms of the eigenmodes:

$$u'(\tau_\star) = \sum_j u'^{(j)}(\tau_\star)\psi^{(j)}, \qquad f = \sum_j f^{(j)}\psi^{(j)}. \quad (32)$$

It then follows from (30) that

$$u'^{(j)}(\tau_\star) = \frac{\mathrm{e}^{\lambda_j \tau_\star} - 1}{\lambda_j} f^{(j)}, \quad (33)$$

in which it is understood that the fraction takes the value $\tau_\star$ when $\lambda = 0$. An important role is played by those eigenvalues for which

$$|\lambda_j|\tau_\star \sim 1; \quad (34)$$

these will be called *threshold eigenvalues*. Since $\tau_\star \propto {K_{\mathrm{G}}}^{-2/3}$ there is a whole range of eigenvalues well below and well above the threshold. The corresponding eigenmodes will be called "low-lying" and "high-lying" modes, respectively. Well below threshold the fraction in (33) can be Taylor expanded, yielding to leading order $\tau_\star f^{(j)}$: those modes are essentially unaffected by their interaction with the flow through the Orr–Sommerfeld operator A. We have checked that such modes are responsible for the low-amplitude oscillatory tail to the left of the boundary layer seen in Fig. 16. Well above threshold, the modulus of the fraction is much smaller than $\tau_\star$ because $\mathrm{e}^{\lambda_j \tau_\star}$ is essentially a phase factor [51] and one can thus suspect that high-lying modes do not contribute much to the boundary layer. Making this argument solid requires a better control over the phases than we have been able to achieve analytically. We have thus carried out numerically partial summations of the r.h.s. of (32), on the one hand starting from low-lying eigenmodes and adding progressively higher-lying eigenmodes and on the other hand doing it in reverse. In both instances we found that the boundary layer of Fig. 16 emerges mostly from modes near the threshold [52].

When (33) is applied near threshold, the $1/\lambda_j$ yields a factor $\tau_\star \propto {K_{\mathrm{G}}}^{-2/3}$, while the beating input has an overall factor $\propto {K_{\mathrm{G}}}^{-1/3}$. Together, this produces a ${K_{\mathrm{G}}}^{-1}$ amplitude factor in a boundary layer of thickness $\propto {K_{\mathrm{G}}}^{1/3}$, needed to explain the ${K_{\mathrm{G}}}^{-2/3}$ law for the amplitude of the $t = t_\star$ tyger in physical space. What we just explained is however far from a proof since (i) we did not show analytically that the dominant contribution to the boundary layer comes from threshold modes and (ii) a ${K_{\mathrm{G}}}^{-1}$ amplitude factor for the beating input f does not necessarily imply the same factor for its threshold components $f^{(j)}$.

IV. OPEN PROBLEMS AND CONCLUSION

We must now conclude our adventures in Tygerland. Although this project has been unfolding over three years, we have the feeling that we only indented the subject, as far as true mathematical understanding is concerned. For example in Sec. III, devoted just to the birth of tygers, we have not identified analytically the important mechanism which allows threshold modes to populate the boundary layer seen in Fig. 16.

As to the after-birth events, they have so far only been the subject of numerical experimentation and occasional phenomenological theory. The collapse of the tyger, shortly after the time of appearance of the first shock, seen in Fig. 5 is strongly reminiscent of the collapse phenomenon in plasmas [31]. The immediately subsequent development, as we have seen in Sec. II B, involves at least two phenomena. One is the spreading out on the ramp, the moving of the tyger along the ramps of the untruncated Burgers solution, which perhaps can be explained by advection effects; the other one is that the small-scale motion looses the highly organized structure seen around $t_\star$; in other words the Fourier spectrum broadens away from the Galerkin wavenumber. This may signal the onset of the thermalization of the solution which, eventually, becomes a Gaussian noise in the space variable with a flat spectrum. Here a digression is in order. The ordinary untruncated Burgers equation—with or without viscosity—has played a major role, not only as testing ground for numerical schemes, but also for helping us to find mistakes in excessively naive ideas intended for Navier–Stokes turbulence. The Galerkin-truncated Burgers equation may take us a step further, being paradoxically closer to Euler–Navier–Stokes: it is nonlocal (in a way consistent with energy conservation) and its solutions display spatio-temporal chaos, as documented, e.g., in [15].

Of course all this would be quite academic if we did not already have good evidence that the key phenomena associated to tygers are also present in the two-dimensional incompressible Euler equation, as discussed in Sec. II C. Our understanding of this, so far, based on what we know about the analytic structure of 2D flow, is far from complete. It seems important to find out how the more systematic theory of the birth can be carried over to 2D—and perhaps 3D—Euler. So far, it is clear that complex-space singularities approaching the real domain within one Galerkin wavelength are the triggering factor, as in the 1D Burgers case.

Now, a few remarks about tyger purging, which is definitely not the central issue of the present investigation. We have seen in Sec. II that tygers, being born far from shocks, do not modify shock dynamics but do modify the flow else-

where because the tygers induce Reynolds stresses on scales much larger than the Galerkin wavelength; hence the weak limit of the Galerkin-truncated solution as $K_{\rm G} \to \infty$ is definitely not the inviscid limit of the untruncated solution. Can we "purge tygers away" and thereby obtain a subgrid-scale method which describes the inviscid-limit solution right down to the Galerkin wavelength?

How to do this practically? Several ideas come to mind. One is simply to apply some amount of viscosity. If the viscosity is sufficiently large, the truncation becomes irrelevant but the solution thus obtained will not coincide with the inviscid limit down to the Galerkin wavelength or anywhere close to it. A second idea is to look for embryonic tygers in physical space and selectively abort them. This can perhaps be done by a suitable wavelet or filtering technique but may be tricky [53]. A simpler idea is to purge the boundary layer near $K_{\rm G}$ at each time step. However this amounts to applying a Galerkin truncation with a slightly smaller $K_{\rm G}$ and will produce more tygers. A more subtle way worth exploring is to wait until a low amplitude tyger has appeared that is concentrated in a sufficiently narrow boundary layer near $K_{\rm G}$ [54] and then to perform the purging, an operation which clearly should not take place too often. Such ideas will of course have to be tested carefully in future work. One may also wonder to what extent such a purging technique can be carried over to 2D and 3D incompressible flow. We have already checked that for the case of 2D and 3D incompressible flow, the birth of the tyger takes place in a narrow boundary layer near the Galerkin truncation.

ACKNOWLEDGMENTS

We are most grateful to the late Steven A. Orszag who introduced us to spectral methods. We had many useful discussions, in particular with C. Bardos, J. Bec, S. Bhattacharjee, M. Blank, M.E. Brachet, P. Constantin, H. Frisch, J. Goodman, J.-L. Guermond, K. Khanin, A. Majda, R. Nguyen Van Yen, R. Pandit, R. Pasquetti, W. Pauls and J.-Z. Zhu.. Computations used the Mésocentre de calcul of the Observatoire de la Côte d'Azur and the SX-8 at the Yukawa Institute of Kyoto University and SERC (IISc). UF's and SSR's work was supported in part by COST Action MP0806 and by ANR "OTARIE" BLAN07-2_183172. TM's work was supported by the GCOE Program "The Next Generation of Physics, Spun from Universality and Emergence" from the MEXT of Japan. SSR acknowledges DST (including its coming Indo-French IFCAM program) and UGC (India) for support. SN and TM thank the French Ministry of Education for funding several extended visits to the Observatoire de la Côte d'Azur.

Appendices

Appendix A: Numerics and graphical representation

With the exception of the inviscid-limit solutions of the untruncated Burgers equation which were obtained by the Fast Legendre Transform method [33], all the numerical simulations presented in this paper used the pseudo-spectral method [9], in combination with a fourth-order Runge–Kutta time marching with a time step 10^{-4} for $K_{\rm G} \leq 5,000$ and 10^{-5} for $K_{\rm G} > 5,000$. Up to 2^{16} collocation points were used. In order to implement Galerkin truncation it was essential to remove aliasing. In principle this can be done by the so-called two-thirds rule: $K_{\rm G} \leq (2/3)K_{\rm max} = N/3$, where N is the number of collocation points. This allows a calculation of the solution at collocation points which suffers only from double-precision rounding errors and temporal truncation.

However, when it comes to representing tygers graphically, using the two-thirds rule can produce a stroboscopic graphical artefact, illustrated in Fig. 18. Since in the presence of tygers there is a strong excitation at and near the truncation wavenumber $K_{\rm G}$, the velocity is very close to a sine wave with Galerkin wavelength. Unless proper interpolation is used, such a sine wave cannot be correctly represented using only three points per wavelength. Otherwise the rapid oscillations disappear in favor of an illusory triple valuedness. One easy way to do the interpolation is to use a much higher number of collocation points whenever graphical output is needed.

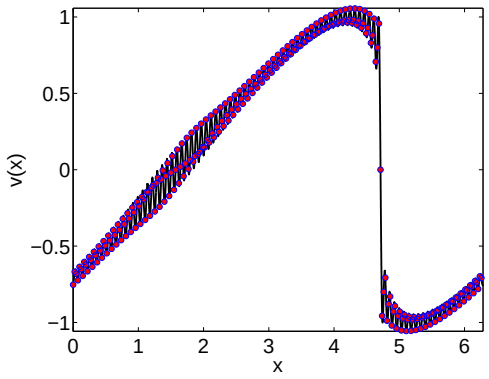

FIG. 18: (Color online) Plots of the solution $v(x)$ of the Galerkin-truncated Burgers equation, with $K_{\rm G} = 85$, using two different numbers of collocation points, namely, $N = 16,384$ (black continuous line) and with red-filled circles (black circles) for $N = 256$ for the single-mode initial condition $v_0(x) = \sin(x - \pi/2)$ shown at time $t = 1.10$. This plot illustrates the stroboscopic effect, a purely graphical interpolation artefact, caused by insufficient resolution for a given $K_{\rm G}$.

Appendix B: Real and complex singularities for the Burgers equation

As is well known, the solutions of hydrodynamical equations such as the Burgers or Euler equations in any dimension with space-periodic and analytic initial data, remain so for at least a finite time (cf., e.g., Refs. [10, 11] and references therein). In the 1D Burgers case, a real singularity appears after a finite time (finite-time blow up). For 2D Euler, analyticity is preserved for all times but complex-space singularities will typically approach the real domain arbitrarily close at long times. For 3D Euler it is not clear if there is or not finite-time blow up. The signature of complex-space singularities—more

precisely of those closest to the real domain—is an exponential fall-off at high wavenumbers k of the spatial Fourier transform $\propto \mathrm{e}^{-\delta(t)k}$ (within algebraic prefactors), where $\delta(t)$ is the width of the analyticity strip, that is the distance from the real domain of the nearest complex-space singularity. As long as $\delta(t)K_{\mathrm{G}} \gg 1$ the effect of Galerkin truncation is exponentially small and can be ignored for all the purposes of the present study. For convenience we define the threshold as the time t_{G} when $\delta(t_{\mathrm{G}})K_{\mathrm{G}} = 1$.

Let us here recall how $\delta(t)$ can be obtained explicitly for the case of the untruncated Burgers equation with the initial condition $u_0(x) = -\sin x$ (for details, cf. Ref. [16]). In Lagrangian coordinates, the motion of an inviscid Burgers fluid particle is given by

$$a \mapsto x = a + tu_0(a) = a - t\sin a. \tag{B1}$$

A singularity is obtained when the Jacobian $\partial x/\partial a$ of this map vanishes. For t slightly less than $t_\star = 1$, the Lagrangian and Eulerian locations of the singularity nearest to the real domain is close to the origin and can be obtained by expanding $\sin a$ to cubic order. We thus have, up to higher-order terms:

$$x = (t_\star - t)a + \frac{a^3}{6}; \quad \partial x/\partial a = t_\star - t + \frac{a^2}{2}. \tag{B2}$$

The Jacobian is seen to vanish at $a_\star(t) = \pm\mathrm{i}\sqrt{2(t_\star - t)}$. The corresponding Eulerian singularities are at

$$x_\star(t) = \pm\frac{2\sqrt{2}}{3}\mathrm{i}(t_\star - t)^{3/2}. \tag{B3}$$

Equating the modulus $\delta(t)$ of the imaginary part of $x_\star(t)$ to $1/K_{\mathrm{G}}$, we obtain:

$$t_\star - t_{\mathrm{G}} = \left(\frac{3}{2\sqrt{2}}\right)^{2/3} {K_{\mathrm{G}}}^{-2/3} \approx 1.04{K_{\mathrm{G}}}^{-2/3}. \tag{B4}$$

For convenience we have replaced 1.04 by unity and thus used in Sec. III

$$t_{\mathrm{G}} = t_\star - {K_{\mathrm{G}}}^{-2/3}. \tag{B5}$$

Appendix C: The beating input

Our purpose it to find the large-K_{G} asymptotic behavior of the beating input (28), repeated here for convenience,

$$\hat{f}_k \equiv \mathrm{i}k \sum_{p+q=k} (\hat{u}^<_{\star p}\,\hat{u}^>_{\star q} + \frac{1}{2}\hat{u}^>_{\star p}\,\hat{u}^>_{\star q}), \tag{C1}$$

in the range $1 \ll K_{\mathrm{G}} - k \ll K_{\mathrm{G}}$. Although it is this input which eventually permits the birth of the tyger, the beating input is strongest at the preshock and it is best to place the origin there. The function $u_\star$, whose high- and low-passed filtered Fourier transforms appear in (C1), is odd and has a cubic root singularity at the origin. Hence its Fourier transform is pure imaginary, odd and given to leading order at large wavenumbers by

$$\hat{u}_k = \mathrm{i}Ck^{-4/3}, \tag{C2}$$

where C is a real constant and it is understood that $k^{-4/3}$ has the same sign as k. Actually, (C2) is a very good representation of the Fourier transform of $\hat{u}_k$ at all but a few low-lying wavenumbers. Observe that the r.h.s. of (C1) has two terms, the first has $|p| \le K_{\mathrm{G}}$ and $|q| > K_{\mathrm{G}}$ while the second has both $|p|$ and $|q|$ greater than K_{G}. The latter is easily bounded in modulus by $D|k|{K_{\mathrm{G}}}^{-5/3}$ where D is a positive constant and thus will be seen to contribute negligibly to the asymptotics. Hence, from (C1) and (C2), we have

$$\hat{f}_k \;\simeq\; -C^2\mathrm{i}kg_k \tag{C3}$$

$$g_k \;\equiv\; \sum_{p+q=k,\,|p|\le K_{\mathrm{G}},\,|q|>K_{\mathrm{G}}} p^{-4/3}q^{-4/3}. \tag{C4}$$

We introduce dimensionless variables:

$$\tilde{p} \equiv -\frac{p}{K_{\mathrm{G}}}, \quad \tilde{q} \equiv \frac{q}{K_{\mathrm{G}}}, \quad \tilde{k} \equiv \frac{K_{\mathrm{G}} - k}{K_{\mathrm{G}}}, \tag{C5}$$

and rewrite (C4) as

$$g_k = -{K_{\mathrm{G}}}^{-8/3} \sum_{\tilde{k}<\tilde{p}\le 1} \tilde{p}^{-4/3}(1 + \tilde{p} - \tilde{k})^{-4/3}, \tag{C6}$$

where the summation on $\tilde{p}$ is over integer multiples of $1/K_{\mathrm{G}}$. Now we set

$$y \equiv \frac{\tilde{p} - \tilde{k}}{\tilde{k}} \tag{C7}$$

and approximate the summation by an integral to obtain, to leading order,

$$g_k \simeq -\frac{1}{3}{K_{\mathrm{G}}}^{-4/3}(K_{\mathrm{G}} - k)^{-1/3}, \tag{C8}$$

whence

$$\hat{f}_k \simeq \mathrm{i}\frac{1}{3}C^2{K_{\mathrm{G}}}^{-1/3}(K_{\mathrm{G}} - k)^{-1/3}, \quad 1 \ll K_{\mathrm{G}} - k \ll K_{\mathrm{G}}. \tag{C9}$$

There are also subleading corrections involving $(K_{\mathrm{G}} - k)^0$, $(K_{\mathrm{G}} - k)^{+1/3}$, etc [34]. Because the exponent gap is only $1/3$, it is difficult in simulations to see a clean leading order term. Fig. 19 shows the beating input in Fourier space and in physical space.

Appendix D: The Orr–Sommerfeld problem for Galerkin truncation

Here we study the spectral properties of the Orr–Sommerfeld operator governing weak perturbations near the time $t_\star = 1$ of the first singularity of the untruncated solution for the initial condition $u_0 = \sin x$, as introduced in Sec. III.

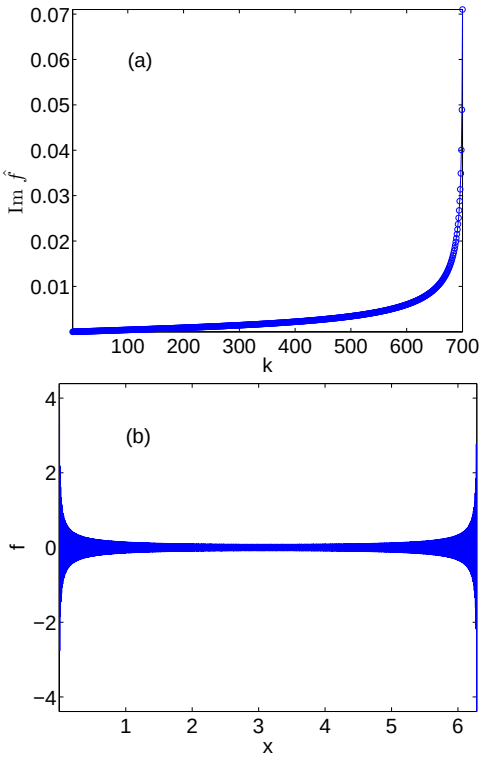

FIG. 19: (Color online) The beating input term, calculated at $t_\star$ and used together with the freezing approximation, evaluated for the single mode initial condition $v_0(x) = u_0(x) = -\sin(x)$ (origin at preshock) for $K_G = 700$. (a): imaginary part in Fourier space; (b): physical space.

This operator involves the Fourier transform $\hat{u}_{\star,\,k}$ of the solution of the untruncated Burgers equation at time $t_\star$. Because this is an odd pure imaginary function of k, we set $\hat{u}_{\star,\,k} = \mathrm{i}\check{u}_k$, where $\check{u}_k$ is a real odd function. With this notation the operator becomes the following real $(2K_{\rm G}+1)\times(2K_{\rm G}+1)$ matrix

$$A_{kk'} \equiv k\,\check{u}_{k-k'}, \quad -K_{\rm G} \le k \le K_{\rm G}, \quad -K_{\rm G} \le k' \le K_{\rm G}. \tag{D1}$$

Indices are integers but not restricted to nonnegative values, unless otherwise stated. Henceforth, unless otherwise stated, all summations are from $-K_{\rm G}$ to $K_{\rm G}$.

We studied the spectral properties of A by standard numerical techniques using MATLAB®, but we also have some analytical results of an algebraic nature. It is appropriate to begin with the latter.

The matrix A is singular, that is it has a vanishing determinant. This is equivalent to stating that there exists a non-vanishing vector (here called a *zero mode*) ψ such that $\sum_{k'} A_{kk'}\psi_{k'} = 0$ for all k. If we can find a ψ such that

$$\sum_{k'} \check{u}_{k-k'}\psi_{k'} = 0, \quad \text{for all } k, \tag{D2}$$

then it follows from (D1) that ψ is also a zero mode of A. The matrix $\check{u}_{k-k'}$ is skew-symmetric and of odd dimension. By an elementary theorem of Jacobi its determinant vanishes and

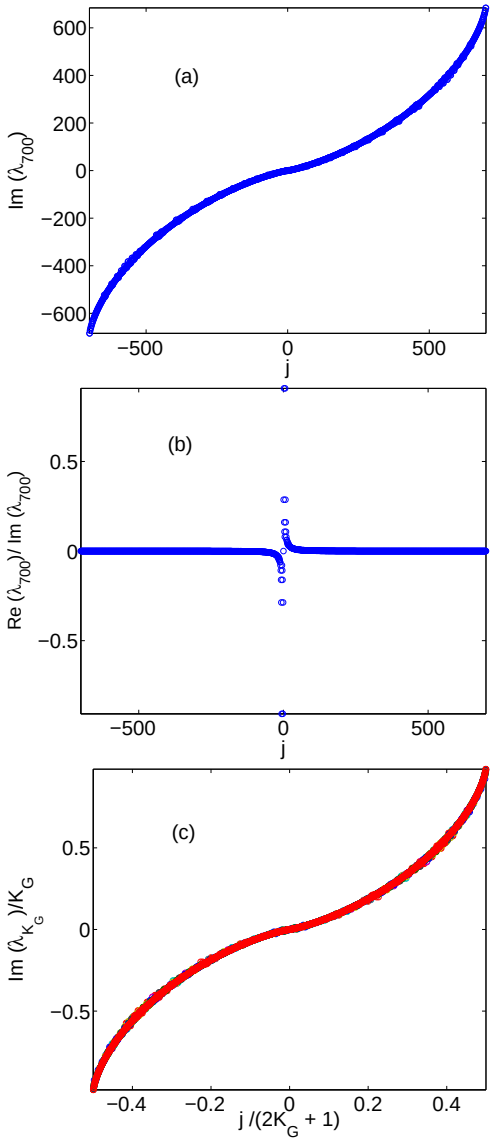

FIG. 20: (Color online) (a): imaginary part of the eigenvalues for $K_{\rm G}$ = 700; (b): ratio of imaginary to real part of the eigenvalues for $K_{\rm G}$ = 700; (c): rescaled imaginary parts of the eigenvalues for $K_{\rm G} = 100,\ 200,\ 300, \ldots,\ 1000$ showing collapse.

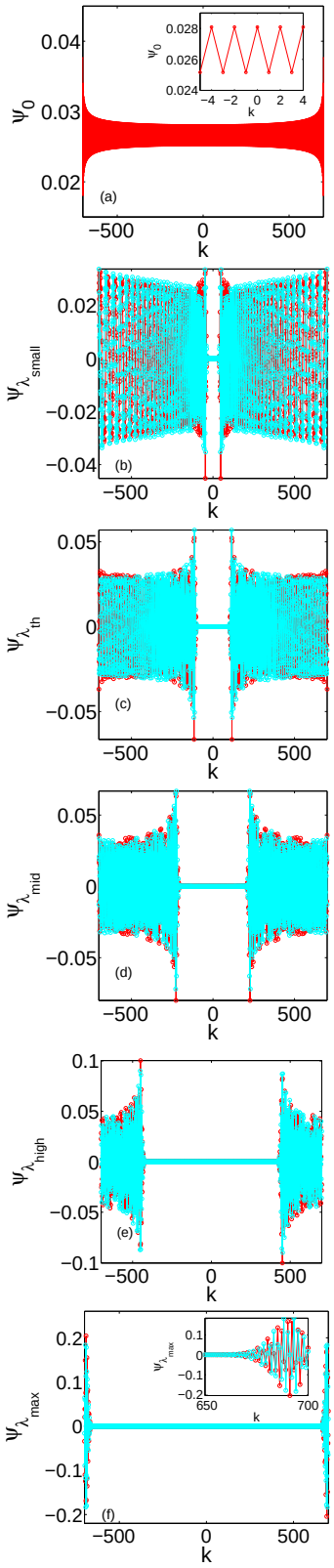

FIG. 21: (Color online) Eigenvectors of the Orr–Sommerfeld operator in Fourier space (origin at the tyger) for $K_{\rm G} = 700$; real parts are shown in red (black) and the imaginary parts in cyan (light grey). (a) modes corresponding to an imaginary part of the eigenvalue which is zero (zero mode, which can be taken purely real), (b) halfway between zero and threshold, (c) at threshold, (d) halfway between threshold and the largest value, (e) close to the largest value, (f) largest value (the inset zooms on the largest wavenumbers).

thus it has a zero mode. Since the entries $\breve{u}_{k-k'}$ are real, the zero mode can also be taken real.

The non-vanishing (complex) eigenvalues come in opposite pairs; the associated eigenvectors which are even or odd in k. The eigenvalue/eigenvector equation for the Orr–Sommerfeld operator A reads

$$\sum_{k'} k\,\breve{u}_{k-k'}\psi_{k'} = \lambda\psi_k \tag{D3}$$

Observe that the operator A (D1) is neither Hermitian nor antihermitian and that, for non-vanishing λ, we have $\psi_0 = 0$. We now exploit the oddness of $\breve{u}_k$, to look for even and odd eigenvectors. First assume that $\psi_k = \psi_{-k}$. In (D3), limiting ourselves to $k > 0$ we separate the k' contributions into positive and negative ones and obtain, using the oddness of $\breve{u}_k$:

$$\sum_{k'=1}^{k'=K_{\rm G}} k\,(\breve{u}_{k-k'} + \breve{u}_{k+k'})\,\psi_{k'} = \lambda\psi_k, \quad k > 0,\ k' > 0. \tag{D4}$$

Now we rescale our eigenvectors by a factor of $1/\sqrt{k}$ [55]:

$$\phi_k \equiv \frac{\psi_k}{\sqrt{k}}, \tag{D5}$$

so as to rewrite the eigenvalue/eigenvector equation as

$$\sum_{k'=1}^{k'=K_{\rm G}} \sqrt{kk'}\,(\breve{u}_{k-k'} + \breve{u}_{k+k'})\,\phi_{k'} = \lambda\phi_k, \quad k > 0,\ k' > 0. \tag{D6}$$

Proceeding similarly under the asumption of an odd eigenvector, we obtain instead of (D6)

$$\sum_{k'=1}^{k'=K_{\rm G}} \sqrt{kk'}\,(\breve{u}_{k-k'} - \breve{u}_{k+k'})\,\phi_{k'} = \lambda\phi_k, \quad k > 0,\ k' > 0. \tag{D7}$$

We now observe that (D6) and (D7) are two eigenvalue/eigenvector equations involving two $K_{\rm G} \times K_{\rm G}$ "reduced" matrices which are negative transposed of each other. Hence their eigenvalues are opposite.

If all eigenvalues of A and of the two reduced matrices are distinct (something for which we have so far only numerical evidence), then the even eigenvectors, the odd ones and the zero mode exhaust the list of $2K_{\rm G} + 1$ eigenvectors of A.

The other results on the spectral properties of the Orr–Sommerfeld operator are obtained numerically (mostly for the case $K_{\rm G} = 700$) and described now, with occasional soft phenomenological interpretations of the findings.

The eigenvalues other than zero are all complex but very close to being pure imaginary. Fig. 20, for the case $K_{\rm G} = 700$, shows the imaginary parts of all 1401 eigenvalues: they range almost exactly from $-K_{\rm G}$ to $K_{\rm G}$. Probably, this is related to the fact that the Orr–Sommerfeld operator (24) is a modified advection operator with an advecting velocity that ranges from -1 to $+1$ and that the k factor which stems from the space derivative cannot exceed $K_{\rm G}$ because of the truncation operator.

The second panel in Fig. 20 shows the ratio of the real to the imaginary part, which is quite small, even for the eigenvalues close to zero. Actually, the real parts can be neglected altogether when used in (33). The explanation may lie in the decomposition of the matrix (D6) into the antihermitian matrix $\sqrt{kk'}\check{u}_{k-k'}$ and the Hermitian matrix $-\sqrt{kk'}\check{u}_{k+k'}$. Remember that in this reduced formulation both k and k' are positive. In the Hermitian part k, k' and $k+k'$ must be less or equal to $K_{\rm G}$. This prevents k and k' from being simultaneously close to $K_{\rm G}$. But we also found that most of the eigenmodes are confined essentially in a relatively narrow boundary layer near $K_{\rm G}$. Hence the Hermitian part cannot contribute much [56].

The third panel in Fig. 20 shows that by simply rescaling by factors $\propto K_{\rm G}$ the horizontal and vertical axes of the distributions of the imaginary parts of the eigenvalues, the curves for different $K_{\rm G}$ all nicely collapse on top of each other, for large enough $K_{\rm G}$, suggesting that some limiting distribution exists as $K_{\rm G} \to \infty$ This we interpret—in highly speculative mode—as follows. Because of the confinement near $K_{\rm G}$ of most of the eigenmodes, we can approximate the reduced matrix $\sqrt{kk'}\check{u}_{k-k'}$ by $K_{\rm G}\check{u}_{k-k'}$, which is $-{\rm i}K_{\rm G}$ times the convolution with the Fourier transform of the velocity $u_\star$. The eigenfunctions of this operator are Dirac measures and the corresponding eigenvalues are $-{\rm i}K_{\rm G}$ times the values the velocity takes at the supports of these Dirac measures.

We now turn to the eigenmodes (Fig. 21). It is seen that the zero mode (first panel: eigenvalue zero) is nearly constant, around 0.0265 with additional small-amplitude even-odd oscillations and some edge effects near $\pm K_{\rm G}$. This structure is not surprising: if it was not for truncation effects, (D2) would be the Fourier transform of the equation $u_\star(x)\psi(x) = 0$ whose solution is an arbitrary linear combination of Dirac measures at the two zeros of $u_\star$, one at the tyger ($x = 0$) and one at the preshock ($x = \pi$). By Fourier transformation, these go over into a constant vector and a vector proportional to $(-1)^k$. As we move to higher eigenvalues, we find that the eigenmodes are localized at higher and higher wavenumbers. This is unexplained but consistent with the almost purely imaginary character of the eigenvalues, as given above.

[1] T.D. Lee, Quart. J. Appl. Math. **10**, 69 (1952).
[2] R.H. Kraichnan, Phys., Fluids **10**, 1417 (1967).
[3] G.L. Eyink and U. Frisch, "Robert H. Kraichnan", in *A Journey through Turbulence in Twelve Chapters* (tentative title), P. Davidson, Y. Kaneda, H.K. Moffatt and K.S.R. Sreenivasan, eds., Cambridge University Press, Cambridge, in press (2010).
[4] R.H. Kraichnan and S. Chen, Physica D **37**, 160 (1989).
[5] C. Cichowlas, P. Bonaïti, F. Debbasch, and M. Brachet, Phys. Rev. Lett. **95**, 264502 (2005).
[6] P.D. Lax and C.D. Levermore, Proc. Natl. Acad, Sci. USA **76** 3602 (1979).
[7] J. Goodman and P.D. Lax, Comm. Pure Appl. Math. **41**, 591 (1988).
[8] T.Y. Hou and P.D. Lax, Comm. Pure Appl. Math. **44**, 1 (1991).
[9] D. Gottlieb and S.A. Orszag, *Numerical analysis of spectral methods: theory and applications*, CBMS-NSF Regional Conference Series in Applied Mathematics **26**, SIAM (1977).
[10] U. Frisch, T. Matsumoto and J. Bec, J. Stat. Phys. **113**, 761 (2003).
[11] J.D. Gibbon, Physica D **237**, 1894 (2008).
[12] E. Hopf, Comm. Pure Appl. Math. **3**, 201 (1950).
[13] P. Constantin, P.D. Lax and A. Majda, Comm. Pure Appl. Math. **38**, 715 (1985).
[14] L.D. Landau, Zh. Eksp. Teor. Fiz. **16**, 574 (1946) [English translation: J. Phys. (Moscow) **10**, 25 (1946)].
[15] A.J. Majda and I. Timofeyev, Proc. Natl. Acad. Sci. USA **97**, 12413 (2000).
[16] J.D. Fournier and U. Frisch, J. Mec. Theor. Appl./J. Theor. Appl. Mech. **2**, 699 (1983).
[17] U. Frisch and J. Bec, "Burgulence", in *Les Houches 2000: New Trends in Turbulence*, M. Lesieur, A. Yaglom and F. David, eds., pp. 341–383, Springer EDP-Sciences (2000).
[18] E. Tadmor, SIAM J. Numer. Anal. **26**, 30 (1989).
[19] R.Z. Sagdeev and A.A. Galeev, *Nonlinear Plasma Theory*, Benjamin, New York (1969).
[20] A.J. Majda and I. Timofeyev, Milan J. Math. **70**, 39 (2002).
[21] E. Fermi, J. Pasta and S. Ulam (with M. Tsingou Menzel), "Studies of nonlinear problems. I" in *Los Alamos report* LA-1940 (1955).
[22] W. Pauls, T. Matsumoto, U. Frisch and J. Bec, Physica D **219**, 40 (2006).
[23] V.I. Yudovich, Chaos **10**, 705 (2000).
[24] C. Bardos and E. Tadmor (private communication).
[25] R. Nguyen Van Yen, M. Farge and K. Schneider, ESAIM: Proc. (EDP Sciences) **29**, 89 (2010).
[26] C. Bardos and E. Tadmor (private communication).
[27] C. Bardos (private communication).
[28] J. Goodman, T. Hou and E. Tadmor, Numer. Math. **67**, 93 (1994).
[29] P.G. Drazin and W.H. Reid, *Hydrodynamic Stability*, 2nd edition, Cambridge University Press, Cambridge (2004).
[30] [http://www.youtube.com/watch?v=l_mp7Wx4b-0]
[31] V.E. Zakharov, Zh. Eksp. Teor. Fiz. **62**, 1745 (1972) [English translation: Sov. Phys. JETP **35**, 908 (1972)].
[32] R. Nguyen Van Yen, M. Farge, D. Kolomenskiy, K. Schneider and N. Kingsbury, Physica D **237**, 2162 (2008).
[33] A. Noullez and M. Vergassola, J. Sci. Comput. **9**, 259 (1994).
[34] H. Frisch (private communication).
[35] In a weak or distributional sense, that is after multiplication by suitable smooth test functions and integrations by parts.
[36] Elementary facts about the solution of the Burgers equation and its singularities are recalled in Appendix B.
[37] The numerical method used to integrate the Burgers equation is described in Appendix A.
[38] A tyger is already seen but not commented upon in the last two panels of Fig. 6.2 of [18]. M.-E. Brachet (Private communication, 2007) was the first to draw our attention to this phenomenon for the case of the initial condition $\sin x$ but did not propose an explanation.
[39] The feeding mechanism producing truncation waves will be analyzed more systematically in Sec. III.
[40] Nonlinear evolution equations for which there is no concept of fluid particle, such as the Constantin–Lax-Majda model [13], do not display the tyger phenomenon.
[41] A semi-discrete scheme is continuous in time and discrete in space.

[42] All the simulations at resolution up to 8192^2 (not shown here) indicate that, just before being affected by truncation, the strongest small-scale activity is in such cigars; they are very thin in the transverse direction and their centerlines have a large radius of curvature; they are located near hyperbolic critical points of the vorticity where there is strong compression in the transverse direction and strong extension in the longitudinal direction.
[43] We also observed in a number of simulations that, before truncation becomes important, critical hyperbolic points of the stream function (stagnation points) and of the vorticity are close to each other; this may be due to having most of the enstrophy concentrated within a relatively narrow wavenumber band.
[44] With much higher precision, truncation effects would become visible.
[45] Evidence for this may be found in [25]. This result was proven recently by Bardos and Tadmor [24].
[46] In contrast to what happens for the Lax–Levermore study of the KdV equation [27].
[47] Actually, at the time of William Blake, the spelling of the animal with a "y" was already obsolete.
[48] Here we mean of course only a property of the Fourier transformation which underlies Heisenberg's proof of the quantum-mechanical uncertainty principle.
[49] This can be done by replacing pairs of successive even-odd Fourier amplitudes by their half differences and their opposites, respectively.
[50] For the case $u_\star = \sin x$, which is not of great relevance here, it may be shown that the eigenvalues of A are pure imaginary. In contrast, for the same velocity but aliased boundary conditions, GHT find a real part equal to $\pm 1/2$.
[51] The real part of the eigenvalues becomes negligibly small for all j when multiplied by $\tau_\star$.
[52] Films of such partial summations are available at [30].
[53] See however an attempt in this direction in Refs. [25, 32].
[54] This may take some time.
[55] Observe that the $1/\sqrt{k}$ rescaling is the k-space analog of the trick used on p. 96 by GHT (in x-space) to prove stability for nonnegative velocities.
[56] For the aliased case of GHT, it seems also that high-lying eigenmodes are confined to such a boundary layer and this may explain why some of their x-space figures are tyger-like.